AD-A097 337 ILLINOIS UNIV AT URBANA COORDINATED SCIENCE LAB F/G 9/3
TERMINATION OF SURFACE ACOUSTIC WAVE VELOCITY AND IMPEDANCE DIF--ETC(
FEB 81 B J HUNSINGER, S DATTA F19628-78-C-0040
UNCLASSIFIED RADC-TR-81-4 NL

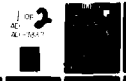

END
DATE FILMED
5-81
DTIC

CINT

LEVEL IV

(12)

(18) (19)

RADC-TR-81-4

Interim Report

(11) Feb 81

(12) 77

(6)

TERMINATION OF SURFACE ACOUSTIC WAVE VELOCITY AND IMPEDANCE DIFFERENCES BETWEEN METAL STRIPS AND FREE SURFACE REGIONS OF METALLIC GRATINGS.

University of Illinois at Urbana-Champaign

(10) B.J. Hunsinger
S. Datta

(9) Interim rept.,

AD A097337

DTIC
SELECTE
APR 6 1981
C

APPROVED FOR PUBLIC RELEASE; DISTRIBUTION UNLIMITED

(15) F19628-78-C-0040

(16) 2305

(17) J5

ROME AIR DEVELOPMENT CENTER
Air Force Systems Command
Griffiss Air Force Base, New York 13441

DTIC FILE COPY

097700

81 4 06 104

This report has been reviewed by the RADC Public Affairs Office (PA) and is releasable to the National Technical Information Service (NTIS). At NTIS it will be releasable to the general public, including foreign nations.

RADC-TR-81-4 has been reviewed and is approved for publication.

APPROVED: Andrew J. Slobodnik, Jr.

ANDREW J. SLOBODNIK, JR.
Project Engineer

APPROVED: Allan C. Schell

ALLAN C. SCHELL, Chief
Electromagnetic Sciences Division

FOR THE COMMANDER: John P. Huss

JOHN P. HUSS
Acting Chief, Plans Office

If your address has changed or if you wish to be removed from the RADC mailing list, or if the addressee is no longer employed by your organization, please notify RADC (EEA), Hanscom AFB MA 01731. This will assist us in maintaining a current mailing list.

Do not return this copy. Retain or destroy.

UNCLASSIFIED

SECURITY CLASSIFICATION OF THIS PAGE (When Data Entered)

REPORT DOCUMENTATION PAGE	READ INSTRUCTIONS BEFORE COMPLETING FORM
1. REPORT NUMBER: RADC-TR-81-4 / 2. GOVT ACCESSION NO.: AD-A097337	3. RECIPIENT'S CATALOG NUMBER:
4. TITLE (and Subtitle): RESEARCH TO PROVIDE A THEORETICAL DETERMINATION OF SURFACE ACOUSTIC WAVE VELOCITY AND IMPEDANCE DIFFERENCES BETWEEN METAL STRIPS AND FREE SURFACE REGIONS OF METALLIC GRATINGS	5. TYPE OF REPORT & PERIOD COVERED: Interim Report
	6. PERFORMING ORG. REPORT NUMBER: N/A
7. AUTHOR(s): B.J. Hunsinger, S. Datta	8. CONTRACT OR GRANT NUMBER(s): F19628-78-C-0040
9. PERFORMING ORGANIZATION NAME AND ADDRESS: University of Illinois at Urbana-Champaign, Coordinated Science Laboratory, Urbana IL 61801	10. PROGRAM ELEMENT, PROJECT, TASK AREA & WORK UNIT NUMBERS: 61102F, 2305J524
11. CONTROLLING OFFICE NAME AND ADDRESS: Deputy for Electronic Technology (EEA), Hanscom AFB MA 01731	12. REPORT DATE: February 1981
	13. NUMBER OF PAGES: 82
14. MONITORING AGENCY NAME & ADDRESS (if different from Controlling Office): Same	15. SECURITY CLASS. (of this report): UNCLASSIFIED
	15a. DECLASSIFICATION/DOWNGRADING SCHEDULE: N/A

16. DISTRIBUTION STATEMENT (of this Report)

Approved for public release; distribution unlimited

17. DISTRIBUTION STATEMENT (of the abstract entered in Block 20, if different from Report)

Same

18. SUPPLEMENTARY NOTES

RADC Project Engineer: Andrew J. Slobodnik, Jr. (EEA)

19. KEY WORDS (Continue on reverse side if necessary and identify by block number)

Surface Acoustic Waves (SAW)
Velocity and Impedance Differences
Metallic Gratings
Elastic Loading
Stored Energy
Piezoelectric Scattering
Periodic Arrays

20. ABSTRACT (Continue on reverse side if necessary and identify by block number)

This interim report describes the scattering theory approach for calculating the shift in velocity and acoustic reflection caused by one electrode (which can be buried) in an infinite array. Piezoelectric loading as well as first and second order mechanical loading are considered. The results calculated from electrode geometry and material constants are presented in the form of scatter matrices from which transmission line model parameters are derived. The analysis is being extended to the finite array case and

DD FORM 1 JAN 73 1473 EDITION OF 1 NOV 65 IS OBSOLETE

UNCLASSIFIED

SECURITY CLASSIFICATION OF THIS PAGE (When Data Entered)

these results will be included in the final report.

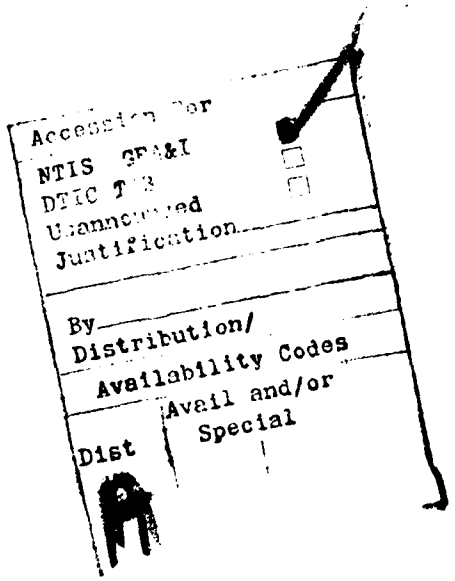

TABLE OF CONTENTS

List of Illustrations

List of Illustrations Cont.

List of Tables

1. INTRODUCTION:

The objective of this three year program is to compute the center frequency transmission line parameters (namely DELTERV and DELTERZ, Ref. 1) for electrodes (including buried electrodes) in a finite length single or double electrode transducer array. These parameters are to be calculated from electrode geometry and material constants taking mass and elastic loading, stored energy, piezoelectric loading and external circuits into effect.

During the first year a full field theory was developed to calculate all of the effects simultaneously. During the present year a different approach was adopted in order to obtain transmission line model parameters that are easily expressed in terms of electrode material and geometry. The scattering process was separated into three categories and each was treated individually using perturbation theory:

*First order Mass and Elastic loading

*Stored Energy Effects (Second order Mass and Elastic loading)

*Piezoelectric loading.

These were first analysed for a single electrode in an infinite array. Section 2 describes the first-order mass and elastic loading analysis and Section 3 describes the analysis of acoustic stored energy scattering. The piezoelectric scattering is analysed in Section 4. This analysis, however, does not allow for interconnections between electrodes and so is not used directly for interdigital transducers. In Section 5 an analytical expression for the frequency response of a single electrode in an infinite grounded array is determined. The results of Sections 4 and 5 have been combined to get a frequency dependent scatter matrix for a single electrode in an infinite array excited with arbitrary voltages on the electrodes. This will be described in the final report. The infinite array analysis for the contract requires the

scattering parameters to be evaluated only at harmonics; however, the finite array analysis presently under development requires the scattering parameters to be evaluated at all frequencies.

All of these scattering contributions are combined to provide a composite mixed unit scatter matrix description for the electrode. The description is left in the scatter matrix form because the transmission line model for odd and even harmonic scattering is different. This scatter matrix is easily converted to the DELTERV and DELTERZ for the odd harmonic transmission line parameters using the equations derived in Appendix I.

2. FIRST ORDER ELASTIC LOADING:

A. Introduction:

The problem of surface wave reflection at thin strip overlays occurs frequently in signal processing devices. Grooved array reflectors employ strip overlays of the same material as the substrate, while metallic transducers incorporate strips of a material different from the substrate. In his book, Auld[2] has described a method for determining the first-order reflection coefficient of a very thin strip overlay. In this method the normal and tangential stresses, T^s_{xy}, T^s_{yy}, T^s_{zy} (Fig. 1b), generated at the interface by the overlay are used as source terms in the normal-mode equation for the generation of the reflected wave. The results, however, when applied to practical cases such as grooves in ST-Z quartz or aluminum on ST-X quartz, yield a value of the reflection coefficient that is too high compared to experimental values.

In Ref.2 , the interface stresses under the overlay T^s_{xy}, T^s_{yy}, T^s_{zy} are assumed to be the same as those due to a uniform overlay extending all along the propagation path. In this section it is shown from the first order equations that, in addition to this uniform component, a pair of delta function shear stresses is generated at the edges of the strip due to its finite extent. The existence of these stresses has also been shown recently by a rigorous perturbation scheme.[8] By incorporating the additional source terms into the normal mode equations, the calculated reflection coefficients for grooves in ST-X quartz and for aluminum on ST-X quartz are found to be in close agreement with observed experimental values. The reflection coefficient calculated for grooves in Y-Z lithium niobate also agrees with the experimental value; however, in this paper any piezoelectric effect due to the overlay is neglected. This effect is negligible in quartz but not necessarily so in lithium niobate.

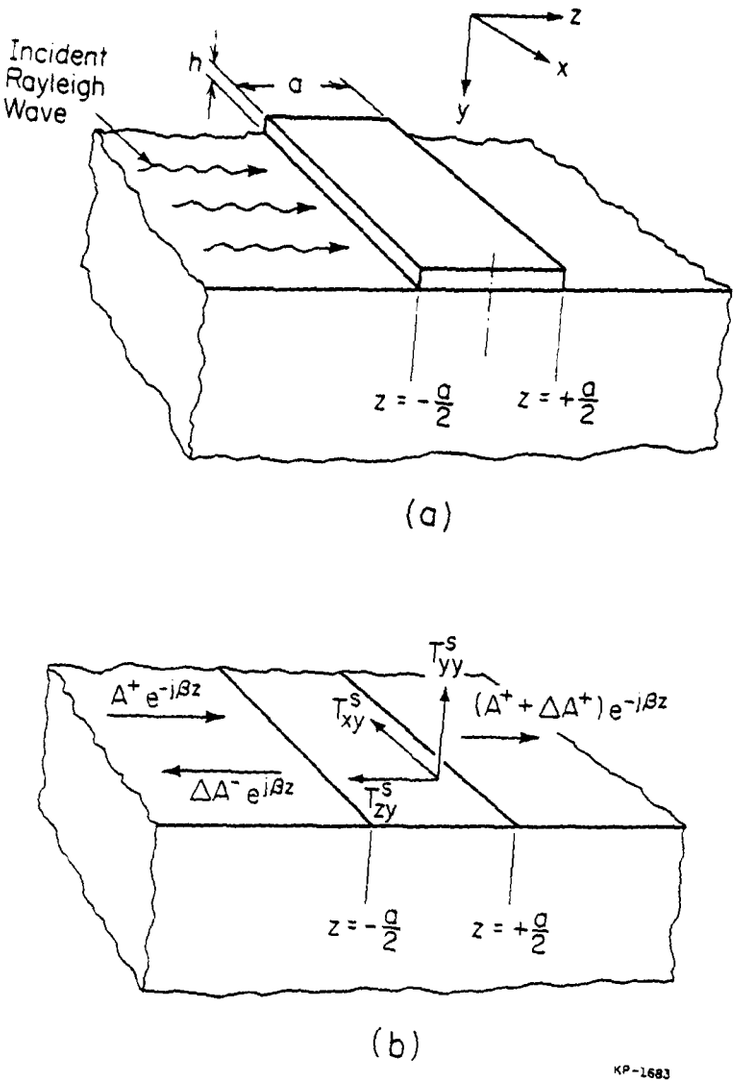

Fig. 1. (a) Incident Rayleigh wave on thin strip overlay.

(b) Generation of reflected wave by stresses generated at strip-substrate interface.

The present formulation thus affords a simple technique for computing the first-order reflection coefficient directly from material parameters.

B. Formulation:

The incident surface wave (Fig. 1a) is assumed to travel in the positive z-direction in a half-space with a free surface so that the surface stresses T_{xy}, T_{yy}, T_{zy} are zero. The wave is uniform in the x-direction and travels with a velocity c_s such that the wave-number β is given by

$$\beta = \omega/c_s$$

where ω is the radian frequency. A thin strip of height h extends along the propagation path from $z = -\frac{a}{2}$ to $z = +\frac{a}{2}$ (Fig. 1a). Due to the presence of the strip, there are interface stresses T^s_{xy}, T^s_{yy}, T^s_{zy} (Fig. 1b) which are the source terms in the normal mode equations[2] describing the change in the incident forward wave and the growth of a reverse wave.

Let A^+ and A^- be the amplitudes of the forward and reverse waves. The surface wave in general has three particle velocity components v_x, v_y, v_z whose values at the surface for the forward wave are written as,

$$v_x = A^+ (v_x^+ e^{-j\beta z}) \tag{1a}$$

$$v_y = A^+ (v_y^+ e^{-j\beta z}) \tag{1b}$$

$$v_z = A^+ (v_z^+ e^{-j\beta z}) \tag{1c}$$

The particle velocities for the reverse wave v_x^R, v_y^R, v_z^R are the negative complex conjugates of those of the forward wave.[3]

$$v_x^R = -A^- (v_x^+ e^{-j\beta z})^* \tag{2a}$$

$$v_y^R = -A^-(v_y^+ e^{-j\beta z})^* \tag{2b}$$

$$v_z^R = -A^-(v_z^+ e^{-j\beta z})^* \tag{2c}$$

The normal mode equations are:

$$\frac{1}{A^+}\frac{dA^+}{dz} = -\frac{1}{|A^+|^2 .4P_a}\left[v_x^* T_{xy}^s + v_y^* T_{yy}^s + v_z^* T_{zy}^s\right] \tag{3}$$

$$\frac{1}{A^-}\frac{dA^-}{dz} = \frac{1}{|A^-|^2 .4P_a} = \left[v_x^{R*} T_{xy}^s + v_{vy}^{R*} T_{yy}^s + v_z^{R*} T_{zy}^s\right] \tag{4}$$

where P_a is the total power per unit beamwidth in a unit amplitude surface wave.

Equation (3) describes the change in velocity of the forward wave. The first order theory to be described here yields the same velocity change as in Ref. 2; so this is not discussed further in this paper. Equation (4) describes the growth of the reflected wave. Using Equations (1) and (2), it is written as,

$$\frac{1}{A^+}\frac{dA^-}{dz} = -\left[z_1\left(\frac{T_{xy}^s}{v_x}\right) + z_2\left(\frac{T_{yy}^s}{v_y}\right) + z_3\left(\frac{T_{zy}^s}{v_z}\right)\right] e^{-j2\beta z} \tag{5}$$

where

$$z_1 = \frac{(v_x^+)^2}{4P_a} \tag{6a}$$

$$z_2 = \frac{(v_y^+)^2}{4P_a} \tag{6b}$$

$$z_3 = \frac{(v_z^+)^2}{4P_a} \tag{6c}$$

Integrating Equation (4) from $z = -\frac{a}{2}$ to $+\frac{a}{2}$ and assuming A^+ to be constant over this region we obtain the reflection coefficient, r.

$$r = \frac{\Delta A^-}{A^+} = z_1 I_x + z_2 I_y + z_3 I_z \tag{7}$$

where,

$$I_x = \int_{-\frac{a}{2}}^{+\frac{a}{2}} \left(\frac{T^s_{xy}}{v_x}\right) e^{-j2\beta z}\, dz \tag{8a}$$

$$I_y = \int_{-\frac{a}{2}}^{+\frac{a}{2}} \left(\frac{T^2_{yy}}{v_y}\right) e^{-j2\beta z}\, dz \tag{8b}$$

$$I_z = \int_{-\frac{a}{2}}^{+\frac{a}{2}} \left(\frac{T^s_{zy}}{v_z}\right) e^{-j2\beta z}\, dz \tag{8c}$$

C. Interface Stresses Generated by Strip Loading:

To obtain I_x, I_y, and I_z, we have to determine the induced stresses T^s_{xy}, T^s_{yy}, and T^s_{zy} at the interface between the strip and the substrate. In the first-order approximation, the particle velocities throughout the strip can be assumed to be the same as those at the surface of the substrate due to the incident wave.[2] The interface stresses are then readily determined by considering the forces acting on a differential element dx dz of the strip of height h. From the x-directed forces (Fig. 2a),

$$T^s_{xy} = j\omega\rho' h v_x - h.\frac{\partial T'_{xz}}{\partial z} . \tag{9a}$$

From the y-directed forces (Fig. 2b),

$$T^s_{yy} = j\omega\rho' h v_y . \tag{9b}$$

From the z-directed forces (Fig. 2c),

$$T^s_{zy} = j\omega\rho' h v_z - h.\frac{\partial T'_{zz}}{\partial z} \tag{9c}$$

where ρ' is the mass-density of the strip.

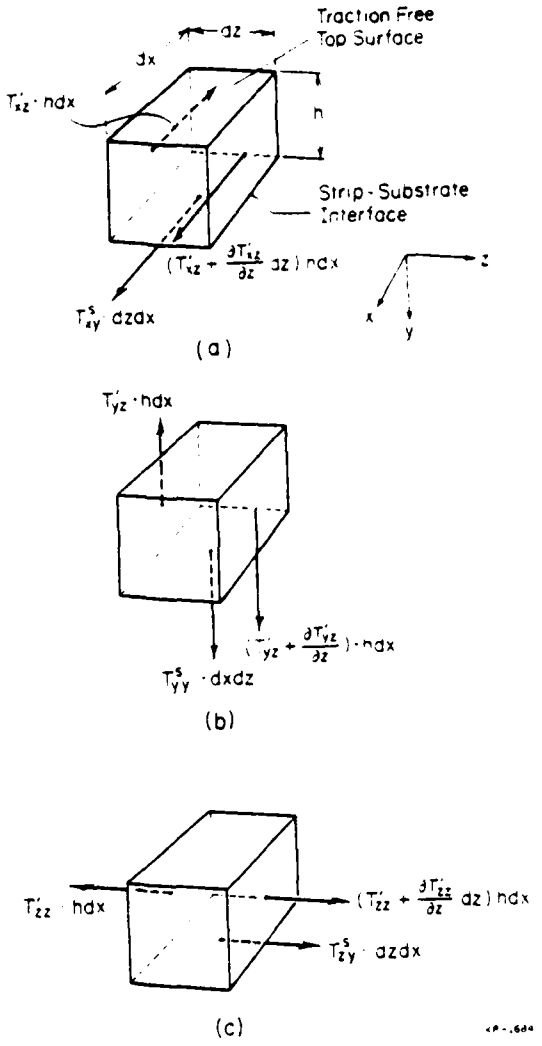

Fig. 2. First-order forces acting on a differential element of the strip in

(a) x-direction

(b) y-direction

(c) z-direction.

T'_{yz} has been neglected in Equation (9b) because its first order value is zero in the strip. The primes are used on T'_{xz}, T'_{yz}, and T'_{zz} to denote that these are fields in the strip rather than in the substrate. These results have also been derived in Ref. 2 using a rigorous Taylor's series expansion for the fields in the strip.

In Equations (9a) and (9c) T'_{xz} and T'_{zz} are the stresses in the strip which is assumed to have the same particle velocities v_x and v_z as the substrate. We may write,

$$T'_{xz} = -\frac{\beta}{\omega} \alpha'_x v_x \tag{10a}$$

$$T'_{zz} = -\frac{\beta}{\omega} \alpha'_z v_z \tag{10b}$$

where α'_x and α'_z are constants with the dimensions of stiffness (nt/m^2). These are effective stiffness coefficients that depend on the material of the strip. In a strip made of an isotropic material with Lame' constants λ' and μ', α'_x, α'_z are readily obtained from the plane strain equations assuming the first order T'_{yy} to be zero.

$$\alpha'_x = \mu' \tag{11a}$$

$$\alpha'_z = \frac{4\mu'(\lambda' + \mu')}{\lambda' + 2\mu'} \tag{11b}$$

For an anisotropic strip equations similar to (11) are derived but are more complicated.[2] However, for an anisotropic strip of the same material as the substrate, T'_{zz} and T'_{zx} are the same as the surface values of these quantities in the incident unperturbed surface wave.

$$T'_{zz} = T_{zz} \tag{12a}$$

$$T'_{xz} = T_{xz} \tag{12b}$$

where T_{zz} and T_{xz} are the surface stress fields of the incident surface wave.

It will be noticed that the derivatives of T'_{xz} and T'_{zz} with respect to z appear in Equations (9a) and (9c). These stresses have a uniform value (multiplied by the factor $\exp[-j\beta z]$) over the entire length of the strip. However, at the end faces ($z = -\frac{a}{2}$ and $z = +\frac{a}{2}$) these stresses must be zero. This leads to the excitation of evanescent modes around each edge which give rise to the second order ($\sim (\beta h)^2$) stored energy effects.[6] In the present first-order approximation we will neglect these evanescent modes and assume that the stresses T'_{xz} and T'_{zz} remain uniform over the length of the strip and abruptly go to zero at the edges. Because of this abrupt change, the derivative terms in Equations (9a) and (9c) give rise to delta function stresses at the two edges. We thus have from Equations (9) and (10),

$$\frac{T^s_{xy}}{v_x} = \frac{j(\beta h)}{c_s}\left[\left(\rho' c_s^2 - \alpha'_x\right) + \frac{\alpha'_x}{j\beta}\left(\delta(z + \tfrac{a}{2}) - \delta(z - \tfrac{a}{2})\right)\right] \tag{13a}$$

$$\frac{T^s_{yy}}{v_y} = \frac{j(\beta h)}{c_s}\left[\rho' c_s^2\right] \tag{13b}$$

$$\frac{T^s_{zy}}{v_z} = \frac{j(\beta h)}{c_s}\left[\left(\rho' c_s^2 - \alpha'_z\right) + \frac{\alpha'_z}{j\beta}\left(\delta(z + \tfrac{a}{2}) - \delta(z - \tfrac{a}{2})\right)\right] \tag{13c}$$

where $c_s = \omega/\beta$ is the velocity of the surface wave.

Fig. 3 shows the spatial distribution of the interface stresses. The delta function components of T^s_{xy} and T^s_{zy} at the edges of the strip were not included in Ref. 1. Inserting the computed stresses from Equations (13) into Equations (8) we get,

$$I_x = \frac{j(\beta h)}{c_s}\left(\rho' c_s^2 + \alpha'_x\right)\frac{\sin\beta a}{\beta} \tag{14a}$$

$$I_y = \frac{j(\beta h)}{c_s}\left(\rho' c_s^2\right)\frac{\sin\beta a}{\beta} \tag{14b}$$

$$I_z = \frac{j(\beta h)}{c_s} \left(\rho' c_s^2 + \alpha_z'\right) \frac{\sin\beta a}{\beta} \qquad (14c)$$

Comparing Equations (13) and (14), it will be noticed that the effect of adding the delta function terms is to change the sign of α_x' and α_z' in Equations (13a) and (13c). Physically, this means a change in the sign of the component of reflection due to stiffness since α_x', α_z' represent stiffness while ρ' represents mass.

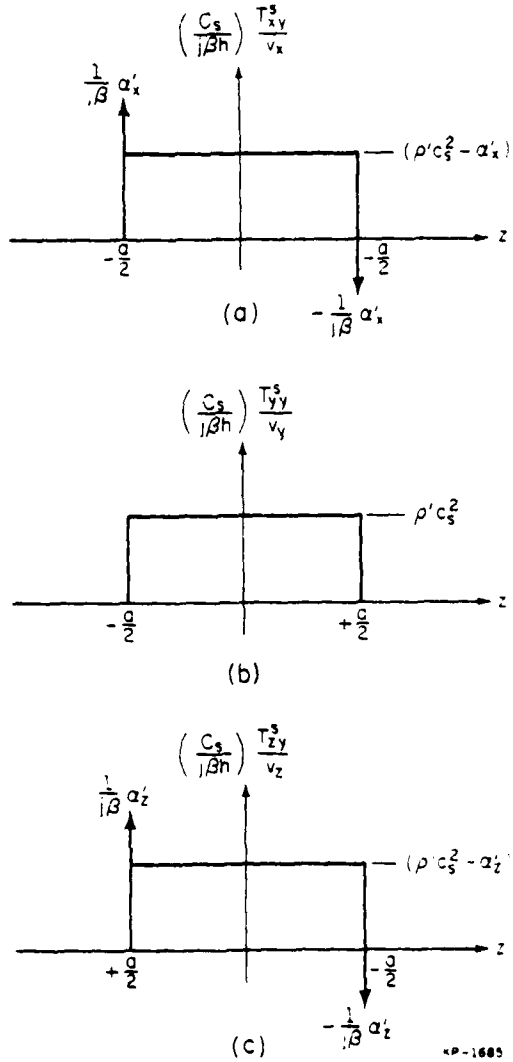

Fig. 3. Spatial distribution of (a) x-directed, (b) y-directed, and (c) z-directed interface stresses.

Combining Equations (14) with Equation (7), we have,

$$r = j\sin\beta a \cdot (\beta h) \left[\rho' c_s^2 \left(\frac{z_1 + z_2 + z_3}{\omega}\right) + \left(\frac{\alpha'_x z_1 + \alpha'_z z_3}{\omega}\right)\right. \qquad (15)$$

D. Application to Specific Cases:

In this section Equation (15) is applied to obtain the first-order reflection coefficients per strip for: (1) aluminum on ST-X quartz and (2) Grooves in ST-X quartz. In each case the computed value closely matches the experimental value reported in Ref. 4.

The values of relevant field quantities at the surface for the unperturbed surface wave in ST-X quartz are given below for a total power per unit beamwidth $P_a = 10^{12}\omega$ Watts/m. These values were computed from the field equations using the method in Ref. 5.

$v_x^+ = .40 \quad \omega < -90°$ m./Sec.

$v_y^+ = 4.24 \quad \omega < +90°$ m./Sec.

$v_z^+ = 2.79 \quad \omega < 0$ m./Sec.

$T_{zz} = 2.42\times10^{11} \quad \beta < 180°$ nt./m.^{2}

$T_{zx} = 2.66\times10^{10} \quad \beta < 90°$ nt./m.^{2}

The mass-density and surface wave velocity for quartz are,

$\rho = 2651$ kg/m.^{3}

$c_s = 3158.5$ m./Sec.

We thus have,

$\frac{z_1}{\omega} = -4\times10^{-14}$ m.^{2}/nt.

$$\frac{z_2}{\omega} = -4.5\times10^{-12} \text{ m.}^2/\text{nt.}$$

$$\frac{z_3}{\omega} = +1.95\times10^{-12} \text{ m.}^2/\text{nt.}$$

Using these values in Equation (15) we get,

$$r = j(\sin\beta a) \cdot \frac{h}{\lambda}\left[-.43\,\frac{\rho'}{\rho} + .0066\,\frac{\alpha_x'}{\rho c_s^2} + .32\,\frac{\alpha_z'}{\rho c_s^2}\right] \qquad (16)$$

This equation gives the reflection coefficient of a strip of any material on ST-X quartz. The strip material is characterized by ρ', α_x', and α_z', ρ being the mass-density of quartz.

(1) Aluminum on ST-X quartz:

Aluminum has Lame' constants λ', μ' and mass-density ρ' equal to,

$$\lambda' = 6.1\times10^{10} \text{ nt./m.}^2$$

$$\mu' = 2.5\times10^{10} \text{ nt./m.}^2$$

$$\rho' = 2695 \quad \text{kg./m.}^3$$

Using Equations (11a) and (11b),

$$\alpha_z' = 7.75\times10^{10} \text{ nt./m.}^2$$

$$\alpha_x' = 2.50\times10^{10} \text{ nt./m.}^2$$

We thus have,

$$\rho'/\rho = 1.017$$

$$\alpha_x'/\rho c_s^2 = 0.945$$

$$\alpha_z'/\rho c_s^2 = 2.930$$

Hence from Equation (16),

$$r = j(\sin\beta a) \cdot (.507 \frac{h}{\lambda})$$

For a reflector array at its fundamental stopband with equal electrode and gap regions, $\sin\beta a = 1$, so that the reflectivity per strip is $.507 \frac{h}{\lambda}$.

(2) Grooves in ST-X quartz:

In this case the overlay is of the same material as the substrate; as discussed in Section C, T'_{zz} and T'_{zx} in the strip may be assumed to be the same as their surface values for the unperturbed waves which are listed at the beginning of this section. Using these values,

$$\alpha'_z = - \frac{\omega}{\beta} \frac{T_{zz}}{v_z} = 8.67 \times 10^{10} \text{ nt./m.}^2$$

$$\alpha'_x = - \frac{\omega}{\beta} \frac{T_{xz}}{v_x} = 6.65 \times 10^{10} \text{ nt./m.}^2$$

We thus have,

$$\rho'/\rho = 1$$
$$\alpha'_x/\rho c_s^2 = 2.514$$
$$\alpha'_z/\rho c_s^2 = 3.278$$

Hence from Equation (16),

$$r = j(\sin\beta a) \ (.636 \frac{h}{\lambda})$$

A similar calculation with Y-Z lithium niobate as the substrate material yields,

$$r = j(\sin\beta a) \cdot \frac{h}{\lambda} \left[- .317 \frac{\rho'}{\rho} + .272 \frac{\alpha'_z}{\rho c_s^2} \right] \qquad (17)$$

where ρ' and α_z' describe the strip material and ρ is the mass-density of lithium niobate ($\rho c_s^2 = 5.72 \times 10^{10}$ nt./m.^{2}). α_x' does not appear in this equation because $v_x = 0$ for a surface in Y-Z lithium niobate. For grooves in Y-Z lithium niobate we have,

$$\alpha_z' = - \frac{\omega}{\beta} \frac{T_{zz}}{v_z} = 2.092 \times 10^{11} \text{ nt./m.}^2$$

so that,

$$\rho'/\rho = 1$$

$$\alpha_z'/\rho c_s^2 = 3.657$$

Equation (14) then yields,

$$r = j(\sin\beta a) \cdot (.678 \frac{h}{\lambda})$$

This result too agrees with experimental data. However, as noted earlier, we have neglected the electrical term in the normal mode equation.

E. Conclusions:

In this section the first-order reflection coefficient of strip overlays on anisotropic substrates is obtained from the well-known normal mode theory. An analytical expression for the reflection coefficient is derived for arbitrary anisotropic strip and substrate materials. The computed values agree well with experimental values for grooves in ST-X quartz and Y-Z lithium niobate and for aluminum on ST-X quartz.

3. STORED ENERGY SCATTERING:

A. Introduction:

The propagation of surface acoustic waves through a periodic array of grooves or thin strip overlays has been modeled[6] as a repetitively mismatched transmission line with reactive energy storage elements (jB) at each discontinuity (Fig. 4). The mismatch parameter $\Delta Z/Z$ has been related to the elastic constants of the substrate and strip material using various theoretical approaches.[7,8,9] However, no theoretical analysis relating the energy storage elements to material constants has yet been described.

The energy storage element (jB) is physically attributed to the excitation of evanescent modes. It is a quadratic effect of order $\sim (h/\lambda)^2$, where h is the height of the strips; this is in contrast to $\Delta Z/Z$ which is a linear effect of order $\sim (h/\lambda)$. This energy storage produces two specific effects on the dispersion curve which have been verified experimentally: (1) it leads to a shift in the center of the fundamental stop-band, and (2) it predicts a stop-band at the second harmonic.

In this section we will describe a model using a first-order perturbation analysis of the strip overlay that predicts these effects and shows their physical origin. Piezoelectric effects are neglected in this paper; only mechanical effects are considered. However, anisotropy is accounted for. The results for a few practical cases involving aluminum electrodes on ST-X quartz and grooves in ST-X quartz are in fair agreement with reported experimental values.

B. Secular Equation:

The field quantities for a wave propagating in a periodic structure satisfy Floquet's Theorem.[10] The particle displacements and the stresses at

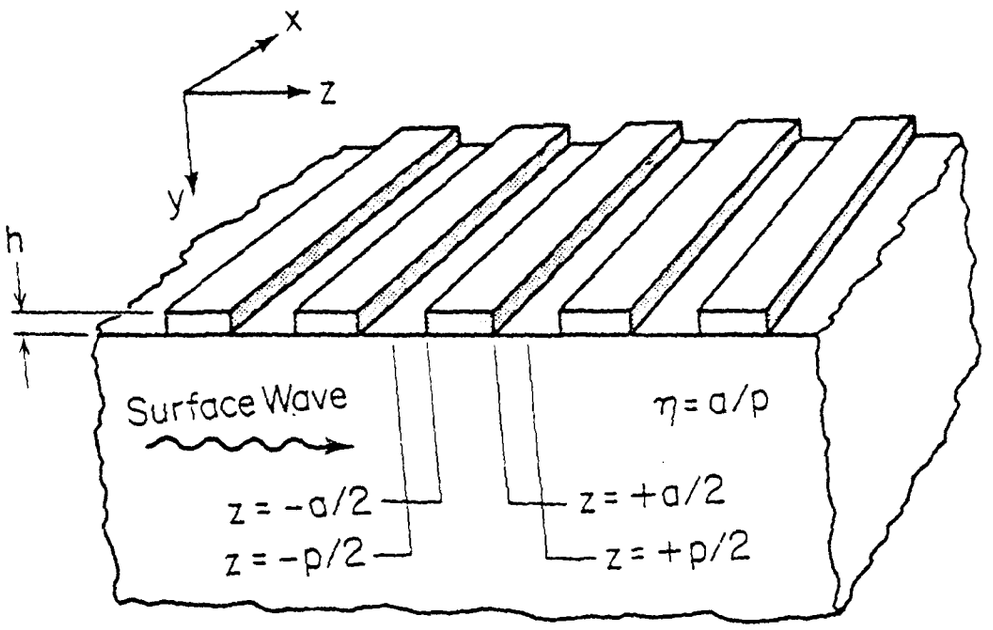

(a)

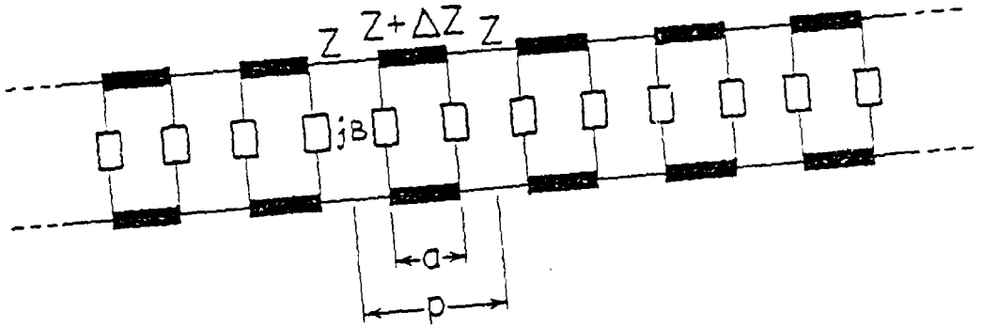

Fig. 4. Surface wave propagation in a periodic array

(a) Physical Structure

(b) Equivalent Circuit

the interface between the layer of strips and the substrate may by written as,

$$U_i = \sum_{n=-\infty}^{+\infty} U_i^{(n)} \exp(-j\beta^{(n)} z) \tag{18a}$$

$$\tau_i = \sum_{n=-\infty}^{+\infty} \tau_i^{(n)} \exp(-j\beta^{(n)} z) \tag{18b}$$

where, $$\beta^{(n)} = \beta + n.2\pi/p \tag{19}$$

p being the period of the strip array. Here τ_i represents the stress at the interface. The second subscript is implied to be y and is dropped for convenience. β is the surface wave wavenumber and $\beta^{(n)}$ represents the n^{th} space harmonic.

The relationship between τ and U required by the periodic array of strips is determined using a first-order perturbation analysis; this analysis is basically similar to that described by Auld in his book[11] with a modification to handle edge effects.[9] Using this analysis, a matrix [L], characteristic of the strip material and geometry (Fig. 5), is evaluated in Appendix II such that,

$$\tau_i^{(m)} = (\beta h) \sum_{n=-\infty}^{+\infty} \sum_{j=x}^{Z} L_{ij}^{(m,n)} U_j^{(n)}, \qquad \begin{matrix} i = x,y,z \\ m = -\infty,\infty \end{matrix} \tag{20a}$$

where h is the height of the strips. A first-order perturbation analysis yields stresses that depend linearly on (βh). The strip array being periodic couples together different space harmonics. A particle displacement at one spatial harmonic, n excites stresses at another spatial harmonic, m.

This is in contrast to the uniform substrate which does not couple different space harmonics. A matrix [S], characteristic of the substrate material (Fig. 5), is evaluated in Appendix III such that,

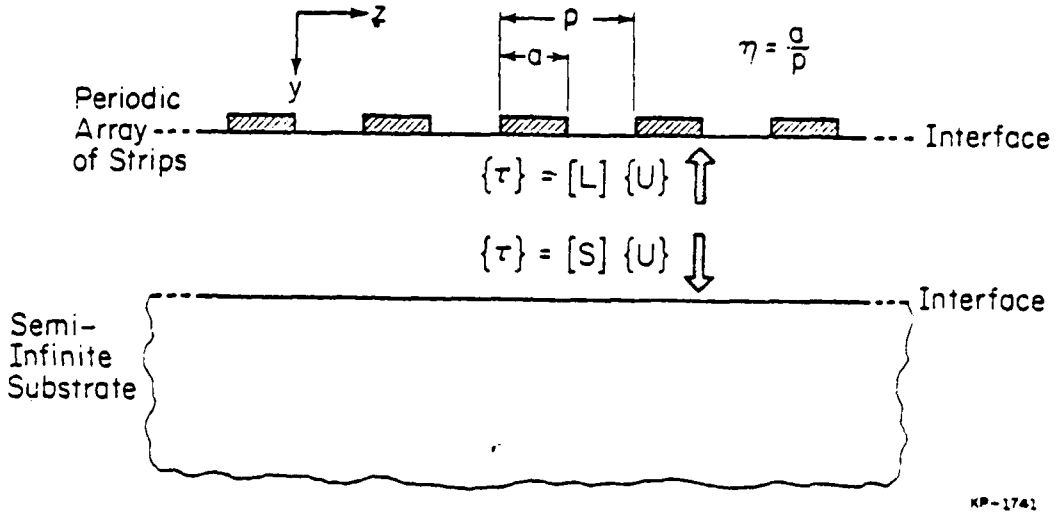

Fig. 5. Stress-displacement relation for a semi-infinite substrate and for a periodic array of strips.

$$\tau_i^{(m)} = \sum_{n=-\infty}^{+\infty} \sum_{j=x}^{z} S_{ij}^{(m,n)} U_j^{(n)}, \qquad \begin{matrix} i = x,y,z \\ m = -\infty,\infty \end{matrix} \tag{20b}$$

Since the uniform substrate does not couple different space harmonics, we have

$$S_{ij}^{(m,n)} = 0 \quad \text{for } m \neq n \tag{21}$$

The [L] and [S] matrices thus describe the elastic properties of the periodic layer of strips and the uniform substrate respectively. The [S] matrix represents an exact analysis of the semi-infinite substrate, while the [L] matrix is based on a first-order perturbation analysis of strips.

The stresses at the interface are equal and opposite for the substrate and the strips, so that equations (20a) and (20b) are combined to yield,

$$\sum_{n=-\infty}^{+\infty} \sum_{j=x}^{z} \left[S_{ij}^{(m,n)} + (\beta h).L_{ij}^{(m,n)} \right] U_j^{(n)} = 0 \qquad \begin{matrix} i = x,y,z \\ m = -\infty,\infty \end{matrix} \tag{22a}$$

In matrix form,

$$\left[[S] + (\beta h).[L] \right] \{U\} = \{0\} \tag{22b}$$

where $\{U\}$ is a 3M x 1 column vector and [S] and [L] are 3M x 3M matrices, if M is the number of space harmonics being considered. The factor 3 arises because of the three dimensions, x, y, and z.

Equation (22b) is the secular equation for the infinite set of space harmonic amplitudes. The elements of [S] and [L] are functions of β and ω so that in principle, one can solve for the dispersion relation $\beta(\omega)$ in any degree of truncation approximation by setting,

$$\det [SL] = 0 \tag{23a}$$

where

$$[SL] = [S] + (\beta h) \, . \, [L] \tag{23b}$$

In the limit $h \to 0$, the strips vanish and there is no coupling between the space harmonics. Equation (23a) then becomes det [S] = 0 and this yields the dispersion curve for surface waves in a substrate with a free surface.

C. Classification of Space Harmonics:

Before we discuss the solutions to equation (23a), it is useful to give a physical interpretation of the different space harmonics. We note that,

$$\beta^{(0)} = \beta \tag{24a}$$

is the wavenumber of the forward propagating surface wave. If β is at one of the stopbands, we may write,

$$\beta = N \cdot \pi/p \tag{24b}$$

where N is an integer. N = 1 represents the fundamental stopband, n = 2 represents the second harmonic stopband and so on. We then have from equation (19),

$$\beta^{(-N)} = -\beta \tag{24c}$$

so that the space harmonic (-N) represents the backward propagating surface wave. As may be expected, at the stopbands the forward and backward waves are coupled together.

Now, the space harmonics with $-N < n < 0$ have $|\beta^{(n)}| < |\beta|$, and thus couple to propagating bulk modes that carry power away from the surface. The space harmonics with $n < -N$ or $n > 0$, on the other hand have $|\beta^{(n)}| > |\beta|$. They couple to evanescent modes that store power reactively near the surface. To summarize:

(1) n = 0 represents the forward wave.

(2) n = -N represents the backward wave.

(3) $-N < n < 0$ represents propagating bulk modes that cause energy loss.

(4) $n < -N$ and $n > 0$ represent evanescent modes that cause energy storage.

This is illustrated in Fig. 6 for N = 3. It will be noted that at the fundamental stopband N = 1 so that there are no space-harmonics in category 3. It is for this reason, we believe, that bulk power losses are much larger for resonators operated at the higher harmoincs than for those operated at the fundamental stopband.

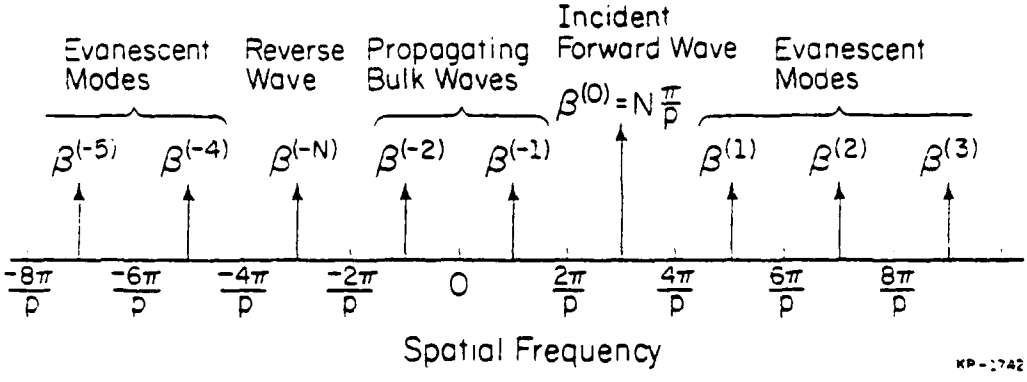

Fig. 6. Spatial harmonics excited by an incident wave in a periodic array at the third harmonic stopband (N = 3).

D. Coupled-Mode Approximation:

In solving Equation (23a) for the secular determinant it is common to use the coupled-mode approximation near a stopband. At the N^{th} stopband the space harmonic amplitudes for n = 0 and n = -N (representing the forward and backward space harmonics) are the largest and only these two are retained. We then write,

$$\det \begin{bmatrix} SL^{(0,0)} & SL^{(0,-N)} \\ SL^{(-N,0)} & SL^{(-N,-N)} \end{bmatrix} = 0 \qquad (25)$$

Here only two space harmonics are retained and the matrix is really 6x6 since 3 dimensions are associated with each space harmonic. Thus $SL^{(0,0)}$, $SL^{(0,-N)}$,

$SL^{(-N,0)}$ and $SL^{(-N,-N)}$ represent (3x3) matrices, but for clarity these are written as single terms.

It will be noted that the off-diagonal terms in Equation (25) come from the periodic strip array. The substrate matrix [S] is zero between different space harmonics. Thus the off-diagonal terms are all of order h/λ. For example,

$$SL^{(0,-N)} = (\beta h) \cdot L^{(0,-N)} \tag{26}$$

since

$$S^{(0,-N)} = 0$$

The dispersion curve can be obtained from Equation (25). Equivalently the normal-mode theory[12] can be used. Either approach yields the mismatch reflection represented by $\Delta Z/Z$, and the results agree with other computations[7,8,9] and with experiment. But this coupled mode approximation does not predict the "stored energy" effect; there is no shift in the centers of the stopbands of order $(h/\lambda)^2$. At the second-harmonic (N = 2), for equal strips and gaps it is found that,

$$L^{(0,-2)} = L^{(-2,0)} = 0 \tag{27}$$

which means that no stopband is predicted at the second harmonic since forward and backward waves are effectively decoupled in this approximation.

It will be noted that carrying the perturbation to second-order in the analysis of the strip-array (that is, in calculating the matrix [L]) does not yield the stored energy effect; there is still no coupling between the forward and backward waves at the second harmonic.

To summarize, the coupled-mode approximation gives us the $\Delta Z/Z$ in the transmission line model, but not $j\beta$ (Fig. 4). Carrying the perturbation analysis of the strips to higher orders only improves $\Delta Z/Z$ to higher orders.

E. Beyond the Coupled-Mode Approximation:

To obtain the "stored energy" effect one needs to go beyond the coupled mode approximation. To illustrate the point, let us include one space-harmonic, n in addition to 0 and -N representing the forward and backward harmonics. Equation (22b) is written as,

$$\begin{bmatrix} SL^{(0,0)} & SL^{(0,-N)} & SL^{(0,n)} \\ SL^{(-N,0)} & SL^{(-N,-N)} & SL^{(-N,n)} \\ SL^{(n,0)} & SL^{(n,-N)} & SL^{(n,n)} \end{bmatrix} \begin{matrix} U^{(0)} \\ U^{(-N)} \\ U^{(n)} \end{matrix} = 0 \qquad (28)$$

From these equations $U^{(n)}$ is eliminated to yield,

$$\begin{bmatrix} SL'^{(0,0)} & SL'^{(0,-N)} \\ SL'^{(-N,0)} & SL'^{(-N,-N)} \end{bmatrix} \begin{matrix} U^{(0)} \\ U^{(-N)} \end{matrix} = 0 \qquad (29)$$

where

$$SL'^{(0,0)} = SL^{(0,0)} - SL^{(0,n)} [SL^{(n,n)}]^{-1} SL^{(n,0)} \qquad (30a)$$

$$SL'^{(0,-N)} = SL^{(0,-N)} - SL^{(0,n)} [SL^{(n,n)}]^{-1} SL^{(n,-N)} \qquad (30b)$$

$$SL'^{(-N,0)} = SL^{(-N,0)} - SL^{(-N,n)} [SL^{(n,n)}]^{-1} SL^{(n,0)} \qquad (30c)$$

$$SL'^{(-N,-N)} = SL^{(-N,-N)} - SL^{(-N,n)} [SL^{(n,n)}]^{-1} SL^{(n,-N)} \qquad (30d)$$

Equation (29) is of the same form as obtained from the coupled-mode approximation but the matrix elements are modified as give by Equations (30). The dispersion curve is obtained by setting,

$$\det \begin{bmatrix} SL'^{(0,0)} & SL'^{(0,-N)} \\ SL'^{(-N,0)} & SL'^{(-N,-N)} \end{bmatrix} = 0 \qquad (31)$$

but now the effect of the space harmonic n is included by using the corrected matrix elements SL' instead of SL.

It will be noted that the correction terms in Equations (30) are each of order $(h/\lambda)^2$ since they contain the product of two off-diagonal terms, each of which is of order h/λ as discussed previously. Moreover, at the second-harmonic stopband $SL'^{(0,-2)} \neq 0$ (though $SL^{(0,-2)} = 0$) because of the extra term in Equation (30b) arising from the additional space harmonic considered. The dispersion curve now shows a shift in the center of the stopband (through $SL'^{(0,0)}$) and also has a stopband at the second-harmonic (through $SL'^{(0,-2)}$). These effects are of order $(h/\lambda)^2$ and arise from the inclusion of the extra space harmonic representing a propagating or an evanescent mode as discussed previously. The corrections in Equations (30) are readily generalized to include as many other space-harmonics as desired:

$$SL'^{(0,0)} = SL^{(0,0)} - \sum_{n,m} SL^{(0,n)}\, G^{(n,m)}\, SL^{(m,0)} \qquad (32a)$$

$$SL'^{(0,-N)} = SL^{(0,-N)} - \sum_{n,m} SL^{(0,n)}\, G^{(n,m)}\, SL^{(m,-N)} \qquad (32b)$$

and similarly for $SL'^{(-N,0)}$ and $SL'^{(-N,-N)}$; where,

$$[G] = [\overline{SL}]^{-1} \qquad (33)$$

$[\overline{SL}]$ being the matrix [SL] with the rows and columns corresponding to 0 and -N deleted. The summation over n,m can be carried out over as many space-harmonics as desired and the total "stored energy" effect is thus obtained.

Equation (31) can then be solved, in principle, to obtain the dispersion curve. Instead we will use the normal mode theory[12] to calculate the phase-shift and the reflection per periodic section. This is simpler to implement than the direct solution of the secular equation.

F. Normal Mode Approach:

In the secular determinant approach, we determine the appropriate ω for a given β so that equation (31) is satisfied. A non-trival solution

$U^{(0)}$, $U^{(-N)}$ is then obtained that satisfies Equation (29). Using the normal mode theory the problem is approached differently. To start with we assume that we have an <u>unperturbed</u> surface wave of amplitude A^+ (Fig. 7). This

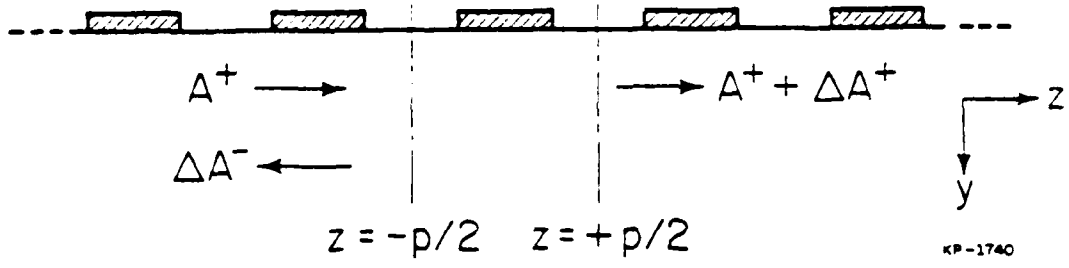

Fig. 7. Surface wave scattering from a single strip in a periodic array.

wave is a normal mode of the semi-infinite medium so that ω and β are related by,

$$\omega = \beta c_S \tag{34}$$

where c_S is the velocity of the surface wave on a free surface. It will be noted that the dispersion relation (34) is a solution of

$$\det [S] = 0 \tag{35}$$

rather than a solution of equation (31).

Since this wave is not a normal mode of the periodic structure, Equation (29) is not satisfied and a residual stress distribution is set up. If the incident forward propagating normal mode has a particle displacement u (u being a vector with three components) then the space harmonics $\tau^{(0)}$ and $\tau^{(-N)}$ of the residual stress are given by,

$$\tau^{(0)} = -SL'^{(0,0)}\, u \tag{36a}$$

$$\tau^{(-N)} = -SL'^{(-N,0)}\, u \tag{36b}$$

This stress distribution now generates a forward wave of amplitude ΔA^+ and a backward wave of amplitude ΔA^- (Fig. 7). ΔA^+ is in quadrature to A^+, leading to a phase-shift of the forward wave; the phase-shift, $\Delta\phi$, per periodic section is given by,

$$\Delta\phi = \Delta A^+/A^+ \tag{37a}$$

and the reflection coefficient, r, per periodic section is given by,

$$r = \Delta A^-/A^+ \tag{37b}$$

$\Delta\phi$ and r are related to the stress t by the normal mode equations:[12]

$$\Delta\phi = \frac{j\omega p}{4P_a} \; u^* . t^{(0)} \tag{38a}$$

$$r = \frac{j\omega p}{4P_a} \; u . t^{(-N)} \tag{38b}$$

where P_a is the power carrier by the normal mode. Using $t^{(0)}$ and $t^{(-N)}$ from Equations (36) and inserting the subscripts running over x,y,z explicitly (which we dropped earlier for convenience), we have,

$$\Delta\phi = -jp \sum_{i,j=x}^{z} SL'^{(0,0)}_{ij} \, Z_{ij} \tag{39a}$$

$$r = -jp \sum_{i,j=x} SL'^{(-N,0)}_{ij} \, Z'_{ij} \tag{39b}$$

where

$$Z_{ij} = \frac{\omega u_i^* u_j}{4P_a} \tag{40a}$$

$$Z'_{ij} = \frac{\omega u_i u_j}{4P_a} \tag{40b}$$

Knowing $\Delta\phi$ and r we can deduce $\Delta Z/Z$ and jB for the transmission line model (Fig. 4). By cascading the transmission matrices of successive periodic

sections, we can then obtain the dispersion relation for the overall array. This normal mode approach gives the same results as the direct solution of the secular equation for small perturbations, but is easier to implement. Moreover it yields the equivalent transmission line parameters directly.

We will now separate the first-order and the stored energy effects in Equations (39) using the expressions for SL' given in Equations (30).

(1) First-order effect:

The first-order effect is obtained from Equations (39) by using only the first term (SL) for SL' from Equations (30). This is the result obtained from the coupled mode approximation. In this approximation we have,

$$\Delta\phi = -j\ (\beta p)\ (\beta h) \sum_{i,j=x}^{z} \frac{L_{ij}^{(0,0)}}{\beta}\ Z_{ij} \tag{41a}$$

$$r = -j\ (\beta p)\ (\beta h) \sum_{i,j=x}^{z} \frac{L_{ij}^{(-N,0)}}{\beta}\ Z'_{ij} \tag{41b}$$

Here we have used SL in place of SL' in Equations (39) and used the fact that (Equation (22a)),

$$\sum_{j=x}^{z} SL_{ij}^{(0,0)}\ u_j = (\beta h) \cdot \sum_{j=x}^{z} L_{ij}^{(0,0)}\ u_j \tag{42a}$$

since

$$\sum_{j=x}^{z} S_{ij}^{(0,0)}\ u_j = 0 \tag{42b}$$

u being the particle displacements of a normal mode for the semi-infinite substrate. In Equation (41b) we have replaced $SL_{ij}^{(-N,0)}$ by $(\beta h) \cdot L_{ij}^{(-N,0)}$ since $S_{ij}^{(-N,0)} = 0$.

Equations (41) show that the phase-shift and reflection obtained from the coupled mode approximation is linear in (h/λ). Using the expres-

sions for L_{ij} from Appendix I this is seen to be the same result as in Reference 9.

(2) Stored energy effect:

The stored energy effect is obtained from Equations (39) by using the second term for SL' from Equations (30):

$$\Delta\phi = j\,(\beta p)\,(\beta h)^2 \sum_{i,j=x}^{z} \frac{H_{ij}^{(0,0)}}{\beta} Z_{ij} \tag{43a}$$

$$r = j\,(\beta p)\,(\beta h)^2 \sum_{i,j=x}^{z} \frac{H_{ij}^{(-N,0)}}{\beta} Z'_{ij} \tag{43b}$$

where

$$H_{ij}^{(0,0)} = \sum_{n,m} \sum_{\ell,k=x} L_{ik}^{(0,n)}\, G_{k\ell}^{(n,m)}\, L_{\ell j} \tag{44a}$$

$$H_{ij}^{(-N,0)} = \sum_{n,m} \sum_{\ell,k=x} L_{ik}^{(-N,n)}\, G_{k\ell}^{(n,m)}\, L_{\ell j}^{(m,0)} \tag{44b}$$

Here [SL] has been replaced by $(\beta h).[L]$ since only the matrix elements between different space harmonics are involved, for which [S] = 0. In Equations (44) the summation over n,m is carried out over as many space harmonics as desired.

The [L] matrix describing the layer is calculated assuming that it is a thin strip uniformly excited across its thickness. This is an invalid assumption at high spatial harmonics, since the penetration depth at the n^{th} harmonic is of order $\sim 1/\beta^{(n)}$. Thus, the matrix element $L^{(m,n)}$ is overestimated by a factor $\beta^{(n)}h$ at high values of n. An exact analysis of a finite thickness strip is rather complicated; a good approximation is to view the strip as a single-mode lossy transmission line in the direction perpendicular to the surface. The transmission line is "shorted" (zero stress) at the top and [L]

represents the "impedance" (stress/displacement) at a distance h from the load. From transmission line theory the impedance Z depends on h through the relation,

$$Z = Z_o \frac{\exp(\beta^{(n)}h) - \exp(-\beta^{(n)}h)}{\exp(\beta^{(n)}h) + \exp(-\beta^{(n)}h)}$$

$$\approx Z_o \beta^{(n)}h \text{ for } \beta^{(n)}h \ll 1$$

where Z_o is some constant and the decay constant along y is assumed equal to $\beta^{(n)}$ for the n^{th} harmonic. The thin strip approximation is valid when $\beta^{(n)}h \ll 1$ and yields an impedance linear in h. An approximate correction for $L^{(m,n)}$ is obtained by multiplying it with the factor,

$$\frac{1}{\beta^{(n)}h} \frac{\exp(\beta^{(n)}h) - \exp(-\beta^{(n)}h)}{\exp(\beta^{(n)}h) + \exp(-\beta^{(n)}h)}$$

This correction factor is clearly not precise; however, the end result is quite insensitive to the precise nature of the correction. This is because the chief contribution to the stored energy effect comes from the lower space harmonics which are unaffected by the factor; the higher space harmonics contribute very little individually. The inclusion of the factor does serve to eliminate spurious contributions arising from the cumulative effect of a large number of space harmonics.

G. Results:

(1) First-order effect (Equations (41)):

Equations (41) give the first-order $\Delta\phi$ and r as obtained from the coupled-mode approximation. Using the expressions for $L_{ij}^{(0,0)}$ and $L_{ij}^{(-N,0)}$ from Appendix I and noting that $\beta = N.\frac{\pi}{p}$, $\Delta\phi$ and r can be evaluated in a straightforward manner. The reflection coefficient is equal to $\Delta Z/Z$ for the transmission line model. The results agree with Reference 9 and the calculations are not repeated here. For grooved arrays, $\Delta\phi$ is found to be zero thus predicting no shift in the stopband center. For electrodes of a material different from the substrate a non-zero $\Delta\phi$ is obtained, but this is of order $\sim (h/\lambda)$ and corresponds to a change in velocity of the wave under the electrode material equal to that due to a uniform layer of the electrode material. Thus, this approximation yields a repetitively mismatched transmission line model with different velocities in the gaps and under the electrodes. The change in wavenumber, $\Delta\beta$, under the electrodes is obtained from $\Delta\phi$ using,

$$\frac{\Delta\beta}{\beta} = \frac{\Delta\phi}{\beta\eta p} \tag{45}$$

where η is the ratio of the electrode width, a, to the period, p (Fig. 5).

(2) Stored energy effect (Equations (43)):

Equations (43) give the $\Delta\phi$ and r due to the stored energy effect.

(i) Phase shift at the fundamental:

The phase-shift at the fundamental was calculated for aluminum electrodes on quartz. We compared our results to the experimental data provided to us by Rome Air Development Center for a double electrode transducer on ST-X quartz. The electrodes were made of 80 Å of chromium and 820 Å of aluminum.

The line width was 1.1729μm corresponding to a fundamental wavelength of 9.3832μm. The fundamental frequency of a double electrode transducer is at half the frequency of the first mechanical stopband. We calculated the change in velocity of the surface wave in propagating under the electrodes. The results are shown in Table I. The piezoelectric effects on ST-X quartz are smaller ($K^2/2$ = .00055) and have been neglected. It is seen that a

Table I: $\Delta v/v$ for a double electrode transducer on ST-X quartz.

Calculated			Measured
1^{st} order	Stored Energy	Total	
.00065	.00385	.0045	.0048

major part of the lowering of velocity is due to the stored energy effect rather than the linear first-order effect.

Figure 8 shows the results for grooves in ST-X quartz with K_v given by,

$$\Delta\phi = (\beta p) \cdot K_v \cdot (h/\lambda)^2 \qquad (46)$$

The experimental points are taken from Reference 13 and show fair agreement. It was pointed out to the author by Melngailis that the large scatter in the experimental data could possibly be due to varying groove shapes; the present analysis assumes a rectangular shape though other shapes can be accounted for by a modification in [L].

The phase-shift for grooves in Y-Z lithium niobate was calculated to be $25(h/\lambda)^2$ at h/λ = .01. This is in agreement with the measured results in Reference 14.

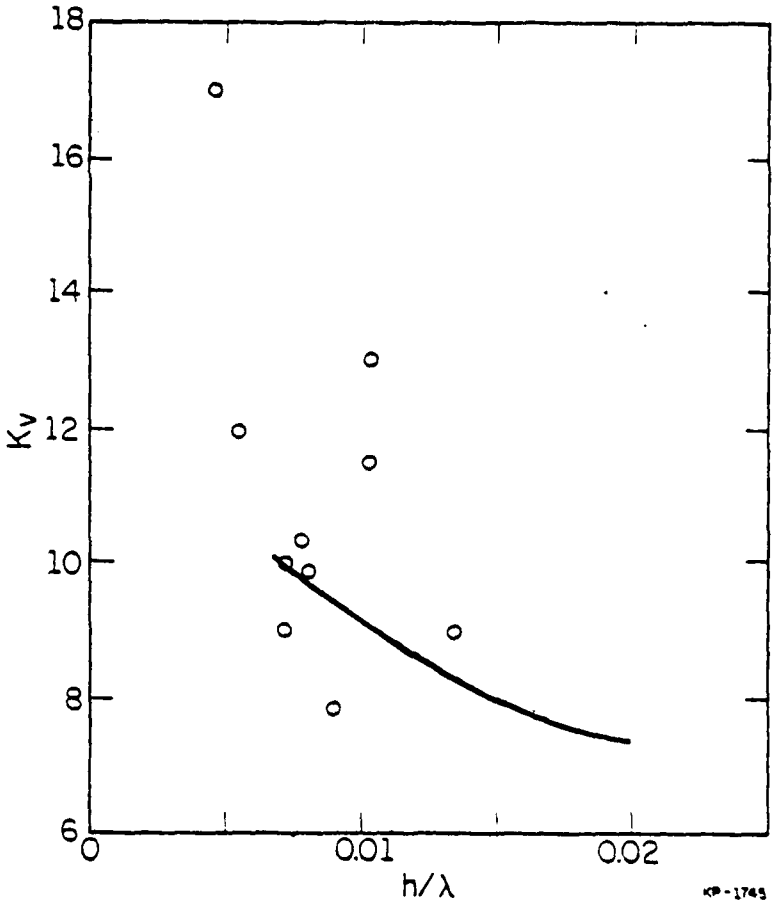

Fig. 8. K_v vs h/λ for grooves in ST-X quartz. Experimental points are taken from Reference 13.

(ii) Reflection at the second harmonic:

The reflection per strip at the second harmonic for grooves in Y-Z lithium niobate was found to be $22(h/\lambda)^2$ at $h/\lambda = .01$ which is about half of the measured value in Reference 6. The reason for this discrepancy is not clear to us.

The reflection coefficient, r per strip was calculated at the second-harmonic stopband for aluminum electrodes on ST-X quartz and for grooves in ST-X quartz. The results are shown in Fig. 9 where K_R is

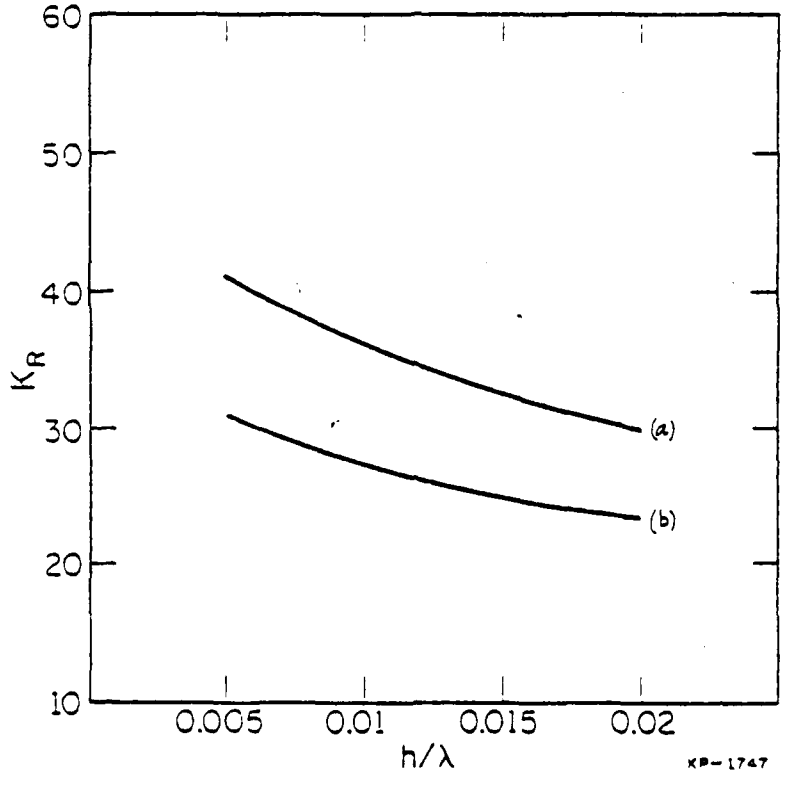

Fig. 9. K_R vs h/λ at the second harmonic for,

(a) Grooves in ST-cut quartz

(b) Aluminum electrodes on ST-cut quartz.

given by,

$$r = K_R \cdot (h/\lambda)^2 \tag{47}$$

This result has not been compared to experimental data.

H. Summary:

A theoretical model for surface wave propagation in a periodic array of thin strip overlays has been developed. The "stored energy" effect is modeled by extending the analysis beyond the coupled mode approximation. The results are discussed for aluminum electrodes and grooves in ST-X quartz and Y-Z lithium niobate.

4. PIEZOELECTRIC SCATTERING:

A. Introduction:

The propagation of surface waves in an infinite periodic array of thin conducting strips has previously been analysed[15-18]; and an equivalent "mixed circuit" model has been obtained[19] by matching dispersion relations near the stop-band. In this section we adopt a different approach that leads directly to the scatter matrix of a single strip in a periodic environment. We assume (Fig. 10) that an unperturbed surface wave is incident on a strip within a periodic array. The incident wave has a surface potential ϕ_s given by,

$$\phi_s = \phi_+ e^{-j\beta z} \tag{48}$$

where β is the wavenumber of the unperturbed wave. The charge induced in the strip by this surface potential is determined from the electrostatic equations. This charge is then used as the source term in the normal mode equations[20] to determine the change in the incident wave, $\Delta\phi_+$ and the generated reverse wave, $\Delta\phi_-$. The scatter matrix describing a strip in a periodic array is thus obtained. Finite arrays (neglecting and effects) are then readily analyzed by cascading the transmission matrices of successive strips. Since the formulation is on a strip by strip basis, assuming local periodicity, slow variations in periodicity and metallization ratio may be accounted for.

The advantages of this approach are:

(1) The scatter matrix of each strip is determined directly at all frequencies so that the model is valid outside the stopbands as well.

(2) Analytical expressions are obtained for each scatter matrix element as a function of metallization ratio and frequency.

(3) The analysis can also be extended to include bulk wave generation by using the charge induced on the strips as the source term in the normal mode equations for the bulk waves.

The formulation presented here is directly applicable to periodic arrays that are electrically periodic as well. This includes open- and short-circuited reflector arrays and multistrip couplers. An extension of the analysis to transducers with the electrodes arbitrarily interconnected is being developed.

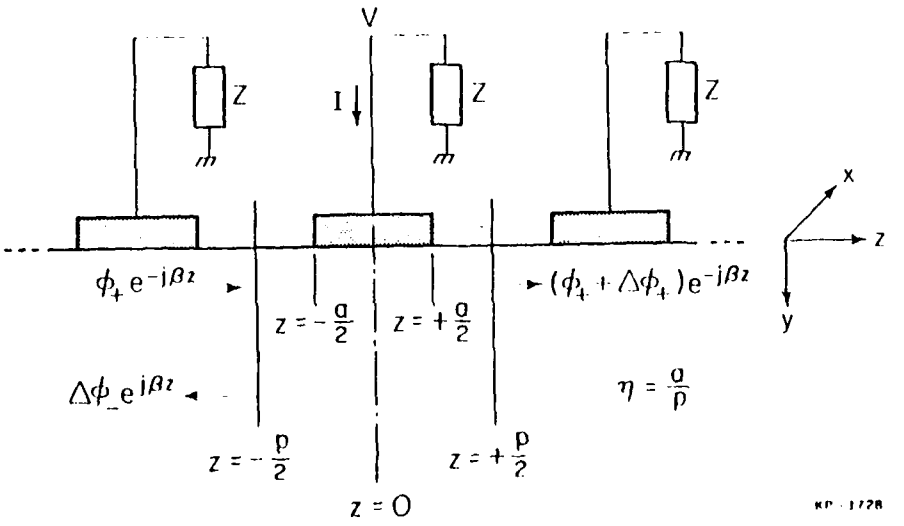

Fig. 10. Reflection and transmission of surface acoustic waves at an electrode in a periodic array.

B. Charge Distribution Induced in a Periodic Array by a Propagating Surface Wave:

In this section we will determine the Fourier components of the induced electrostatic field in a periodic array due to an incident surface wave. For convenience dimensionless variables s, s' and θ are introduced.

$$\theta = \frac{2\pi z}{p} \tag{49a}$$

$$s = \frac{kp}{2\pi} \tag{49b}$$

$$s' = \frac{\beta p}{2\pi} \tag{49c}$$

where, β is the wavenumber of the surface wave

and $\beta = k + N.\ 2\pi/p,$

N being a positive integer such that $0 < k < 2\pi/p$. It follows that,

$$s' = s + N \tag{49d}$$

where $0 < s < 1$.

The surface potential due to the unperturbed wave is given by

$$\phi_s = \phi_+ e^{-j(s+N)\theta} \tag{50a}$$

In the presence of the periodic array of conducting strips an additional electrostatic field is generated. This field is periodic in z and its surface potential ϕ_e is written in a Fourier series as,

$$\phi_e(\theta) = \sum_{n=-\infty}^{\infty} \phi_n e^{-j(s+N)\theta} \tag{50b}$$

The total surface potential is the sum of the wave potential and the induced electrostatic potential.

$$\phi(\theta) = \phi_+ e^{-j(s+N)\theta} + \sum_{n=-\infty}^{\infty} \phi_n e^{-j(s+n)\theta} \tag{51}$$

The tangential electric field, E_z at the surface is obtained from (51)

$$E_z(\theta) = \frac{j2\pi}{p} e^{-js\theta} \left[(s+N)\phi_+ e^{-jN\theta} + \sum_{n=-\infty}^{\infty} (s+n)\phi_n e^{-jn\theta} \right] \quad (52a)$$

The electrostatic part of the field also gives rise to a normal electrical displacement, D_y at the surface (or a charge distribution) that is written from Laplace's equation .

$$D_y(\theta) = \frac{2\pi}{p} (\epsilon_p + \epsilon_o) e^{-js\theta} \left[\sum_{n=-\infty}^{\infty} S_n (s+n)\phi_n e^{-jn\theta} \right] \quad (52b)$$

where, S_n = sign of $(s+N)$

$= +1$ for $n > 0$

$= -1$ for $n < 0$

since $0 < s < 1$.

and ϵ_p is the effective permittivity of the substrate and ϵ_o is the permittivity of the medium above the substrate.

The Fourier coefficients ϕ_n have to be determined such that the boundary conditions imposed by the array are satisfied (Figure 11):

$$E_z(\theta) = 0 \qquad |\theta| < \Delta \quad (53a)$$

$$D_y(\theta) = 0 \qquad \Delta < |\theta| < \pi \quad (53b)$$

where $\Delta = \eta\pi$

η being the metallisation ratio.

These conditions are written from Equation (52a) and (52b) as,

$$e^{-jN\theta} + \sum_{n=-\infty}^{\infty} A_n e^{-jn\theta} = 0 \qquad |\theta| < \Delta \quad (54a)$$

$$\sum_{n=-\infty}^{\infty} S_n A_n e^{-jn\theta} = 0 \qquad \Delta < |\theta| < \pi \quad (54b)$$

where, $A_n = \frac{(s+n)\phi_n}{(s+N)\phi_+}$ (54c)

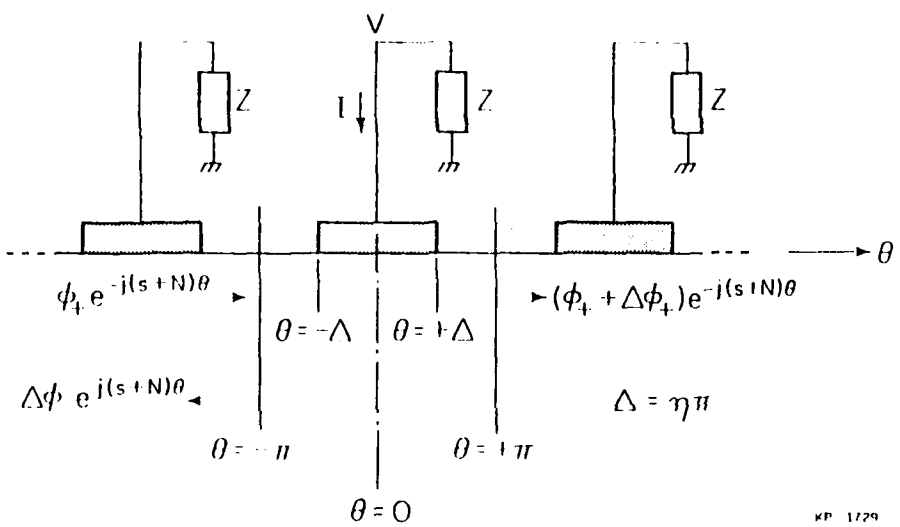

Fig. 11. Same as Figure 10 with dimensionless variables.

It is shown in Appendix IV using the properties of the Legendre polynomial that conditions (54a) and (54b) are satisfied if we write,

$$A_n = \sum_{m=0}^{N} \alpha_m S_n P_{n+m-N-1}(\cos\Delta) + \alpha_{N+1} S_n P_n(\cos\Delta) \qquad (55)$$

where α_{N+1} is any arbitrary number and α_0 to α_N are determined from the following equations:

$$\alpha_0 = -\frac{1}{2} \qquad (56a)$$

$$\alpha_\ell = -\sum_{m=0}^{\ell-1} \alpha_m P_{\ell-m}(\cos\Delta) \ , \ \ell = 1 \text{ to } N \qquad (56b)$$

Here P_n represents the n^{th} Legendre polynomial and P_n for negative n is obtained from the relation $P_{-n-1} = P_n$. The charge distribution in the array is written from Equations (52) and (55),

$$D_y(\theta) = \frac{2\pi}{p} (\epsilon_p + \epsilon_o) e^{-js\theta} \cdot (s+N)\phi_+ \left[\sum_{m=0}^{N+1} \alpha_m \sum_{n=-\infty}^{\infty} P_{n+m-N-1}(\cos\Delta) e^{-jn\theta} \right] \qquad (57)$$

The terminal voltage and current at the strip are shown in Appendix V to be,

$$V = (s+N)\phi_+ \sum_{m=0}^{N+1} (-1)^{N-m+1} \alpha_m \frac{\pi P_{N-m+s}(-\cos\Delta)}{\sin\pi s} \qquad (58a)$$

$$I = j\omega(\epsilon_p + \epsilon_o) W (s+N)\phi_+ \sum_{m=0}^{N+1} \alpha_m \cdot 2\pi P_{N-m+s}(\cos\Delta) \qquad (58b)$$

where W is the length of a strip perpendicular to the direction of wave propagation. α_o to α_N are uniquely known from Equations (56a) and (56b) α_{N+1} has to be chosen so that the correct ratio V/I = Z is obtained from Equations (58a) and (58b).

It is convenient to divide α_{N+1} into two parts:

$$\alpha_{N+1} = \alpha'_{N+1} + \alpha^V_{N+1} \qquad (59)$$

where α'_{N+1} is chosen such that the strip voltage is zero. This corresponds to the case when all the strips are shorted together. From equation (58a),

$$\alpha'_{N+1} = \frac{\sum_{m=0}^{N} (-1)^{N-m} \alpha_m P_{N-m+s}(-\cos\Delta)}{P_{s-1}(-\cos\Delta)} \tag{60}$$

α^{V}_{N+1} is also obtained from Equation (58a):

$$(s+N)\ \mathfrak{D}_+\ \alpha^{V}_{N+1} = \frac{V \sin n\pi s}{\pi\ P_{s-1}(-\cos\Delta)} \tag{61}$$

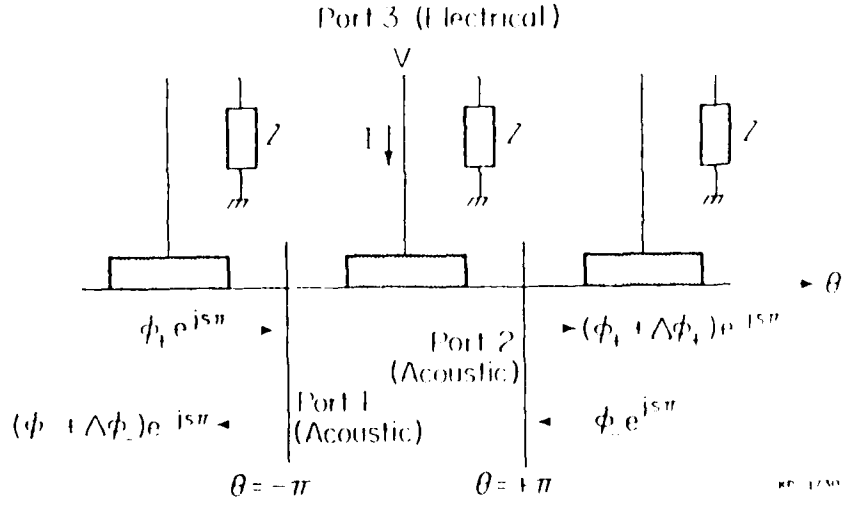

Fig. 12. Scattering at an electrode in a periodic array.

C. Evaluation of Scatter Matrix for a Single Strip:

In this section we will use the induced electrostatic field derived in equations (56) through (61) to obtain the scatter matrix of a single strip. To start with we define a (3x3) matrix A that relates the fields at the two acoustic and one electrical ports (Fig. 12). All values are referenced to the center of the electrode.

$$\begin{Bmatrix} \mathcal{D}_- + \Delta\mathcal{D}_- \\ \mathcal{D}_+ + \Delta\mathcal{D}_+ \\ I \end{Bmatrix} = \begin{bmatrix} A_{11} & A_{12} & A_{13} \\ A_{21} & A_{22} & A_{23} \\ A_{31} & A_{32} & A_{33} \end{bmatrix} \begin{Bmatrix} \mathcal{D}_+ \\ \mathcal{D}_- \\ V \end{Bmatrix} \tag{62a}$$

The (2x2) scatter matrix, S relating the two acoustic ports is easily obtained from the A-matrix by setting

$$I = V/Z \tag{62b}$$

where Z is the external load at each strip. Using equation (62b) in equation (62a) we get,

$$\begin{Bmatrix} \mathcal{D}_- + \Delta\mathcal{D}_- \\ \mathcal{D}_+ + \Delta\mathcal{D}_+ \end{Bmatrix} = \begin{bmatrix} S_{11} & S_{12} \\ S_{21} & S_{22} \end{bmatrix} \begin{Bmatrix} \mathcal{D}_+ \\ \mathcal{D}_- \end{Bmatrix} \tag{63}$$

where,

$$S_{11} = A_{11} - \frac{A_{13}\,A_{31}}{A_{33} - (1/Z)} \tag{64a}$$

$$S_{12} = A_{12} - \frac{A_{13}\,A_{32}}{A_{33} - (1/Z)} \tag{64b}$$

$$S_{21} = A_{21} - \frac{A_{23}\,A_{31}}{A_{33} - (1/Z)} \tag{64c}$$

$$S_{22} = A_{22} - \frac{A_{23}\,A_{32}}{A_{33} - (1/Z)} \tag{64d}$$

We will now evaluate the elements of the A-matrix. The induced electrostatic field was derived in the last section assuming an incident wave only from the left; that is, ϕ_- was set equal to zero. We will thus evaluate the A-matrix elements in the first and third columns (Equation (62a)). The elements in the second column are written from the symmetry of the acoustic ports:

$$A_{12} = A_{21}$$

$$A_{22} = A_{11} \tag{65}$$

$$A_{32} = A_{31}$$

Using equations (58b), (59), (60) and (61) the terminal current, I is written as the sum of two parts--one proportional to ϕ_+ and the other proportional to V. Comparing with equation (62a), we obtain A_{31} and A_{33}.

$$A_{31} = j\omega(\epsilon_p + \epsilon_0)W.2\pi(s+N) \sum_{m=0}^{N} \alpha_m \left(P_{N-m+s}(\cos\Delta) + \frac{(-1)^{N-m} P_{s-1}(\cos\Delta)\ P_{N-m+s}(-\cos\Delta)}{P_{s-1}(-\cos\Delta)} \right) \tag{66}$$

$$A_{33} = 2j\omega(\epsilon_p + \epsilon_0)W.\sin\pi s\ \frac{P_{s-1}(\cos\Delta)}{P_{s-1}(-\cos\Delta)} \tag{67}$$

$A_{31}\phi_+$ represents the strip current with V = 0, that is with the array shorted while $A_{33}V$ represents the strip current due to a voltage V with no incident wave ϕ_+. It will be noted that since the fields were assumed periodic, a voltage V means that the voltage at each strip has the same magnitude V but is delayed in phase with respect to the previous one by $2s\pi$.

Our next step is to evaluate A_{11}, A_{13}, A_{21} and A_{23}. This is done by using the induced charge distribution $D_y(9)$ obtained in the previous section (Equation (57)) to determine the change in the forward wave, $\Delta\phi_+$ and the generated reverse wave, $\Delta\phi_-$ from the normal mode equations:[20]

$$\frac{d\Phi_+}{d\theta} = \frac{jp}{2\pi} \frac{1}{\epsilon_p + \epsilon_0} \left|\frac{\Delta v}{v}\right| \cdot D_y(\theta)\, e^{j(s+N)\theta} \tag{68a}$$

$$\frac{d\Phi_-}{d\theta} = \frac{-jp}{2\pi} \cdot \frac{1}{\epsilon_p + \epsilon_0} \left|\frac{\Delta v}{v}\right| D_y(\theta)\, e^{-j(s+N)\theta} \tag{68b}$$

Integrating over one period from $-\pi$ to $+\pi$ and assuming Φ_+ constant over the period,

$$\frac{\Delta\Phi_+}{\Phi_+} = j\left|\frac{\Delta v}{v}\right| (s+N) \cdot \sum_{m=0}^{N+1} \alpha_m \int_{-\pi}^{+\pi} d\theta \sum_{n=-\infty}^{\infty} P_{n+m-N-1}(\cos\Delta)\, e^{-j(n-N)\theta}$$

$$= j\left|\frac{\Delta v}{v}\right| 2\pi(s+N) \sum_{m=0}^{N+1} \alpha_m\, P_{m-1}(\cos\Delta) \tag{69a}$$

since $\int_{-\pi}^{+\pi} d\theta\, e^{-j(n-N)\theta} = 2\pi$ if $n=N$

$= 0$ otherwise

$$\frac{\Delta\Phi_-}{\Phi_+} = j\left|\frac{\Delta v}{v}\right| (s+N) \sum_{m=0}^{N+1} \alpha_m \int_{-\pi}^{+\pi} d\theta \sum_{n=-\infty}^{\infty} P_{n+m-N-1}(\cos\Delta) e^{-j(2s+n+N)\theta}$$

$$= j\left|\frac{\Delta v}{v}\right| .2\pi(s+N) \sum_{m=0}^{N+1} \alpha_m\, P_{2N+2s-m}(\cos\Delta) \tag{69b}$$

since $\int_{-\pi}^{+\pi} d\theta \sum_{n=-\infty}^{\infty} P_{n+m-N-1}(\cos\Delta) e^{-j(2s+n+N)\theta} = 2\pi \cdot P_{2N+2s-m}(\cos\Delta)$

as shown in Appendix VI. Using Equations (59), (60) and (61) to replace α_{N+1} in equations (69a) and (69b), $\Delta\Phi_+$ and $\Delta\Phi_-$ are written as the sum of two parts--one proportional to Φ_+ and the other proportional to V. This yields the desired A-matrix elements.

$$A_{11} = j\left|\frac{\Delta v}{v}\right| \cdot 2\pi(s+N) \cdot \sum_{m=0}^{N} \alpha_m \left[P_{2N+2s-m}(\cos\Delta) + \frac{(-1)^{N-m} P_{N-m+s}(-\cos\Delta)\ P_{N+2s-1}(\cos\Delta)}{P_{s-1}(-\cos\Delta)} \right] \quad (70a)$$

$$A_{13} = j\left|\frac{\Delta v}{v}\right| \cdot \cdot \frac{2\sin\pi s\ P_{N+2s-1}(\cos\Delta)}{P_{s-1}(-\cos\Delta)} \quad (70b)$$

$$A_{21} = 1 + j\left|\frac{\Delta v}{v}\right| \cdot 2\pi(s+N) \cdot \sum_{m=0}^{N} \alpha_m \left[P_{m-1}(\cos\Delta) + \frac{(-1)^{N-m} P_{N-m+s}(-\cos\Delta)\ P_{N}(\cos\Delta)}{P_{s-1}(-\cos\Delta)} \right] \quad (70c)$$

$$A_{23} = j\left|\frac{\Delta v}{v}\right| \frac{2\sin\pi s\ P_{N}(\cos\Delta)}{P_{s-1}(-\cos\Delta)} \quad (70d)$$

The matrix elements derived earlier are reproduced here for convenience:

$$A_{31} = j\omega(\epsilon_p - \epsilon_0) W \cdot 2\pi(s+N) \cdot \sum_{m=0}^{N} \alpha_m \left[P_{N-m+s}(\cos\Delta) + \frac{(-1)^{N-m} P_{s-1}(\cos\Delta)\ P_{N-m+s}(-\cos\Delta)}{P_{s-1}(-\cos\Delta)} \right] \quad (70e)$$

$$A_{33} = 2j\omega(\epsilon_p + \epsilon_0) W \sin\pi s \frac{P_{s-1}(\cos\Delta)}{P_{s-1}(-\cos\Delta)} \quad (70f)$$

$$A_{12} = A_{21} \quad (70g)$$

$$A_{22} = A_{11} \quad (70h)$$

$$A_{32} = A_{31} \quad (70i)$$

Equations (70) give the complete scatter matrix for a strip in a periodic array once the α_m'S are determined from Equation (56). A few of the α_m'S are calculated here for convenience.

$$\alpha_0 = -\frac{1}{2} \tag{71a}$$

$$\alpha_1 = \frac{1}{2}\cos\Delta \tag{71b}$$

$$\alpha_2 = \frac{1}{4}(\cos^2\Delta - 1) \tag{71c}$$

$$\alpha_3 = \frac{1}{4}(\cos^3\Delta - \cos\Delta) \tag{71d}$$

Equations (64) are used to obtain the scatter matrix of a single strip for a given load termination Z, from the A-matrix derived above.

D. Examples:

We now have analytical expressions for the scatter matrix elements for all frequencies and metallization ratios. In Ref. 19 the reflection coefficient (S_{11}) per strip was computed at various stopbands for open- and short-circuited arrays. In this section we will compare our results with Ref. 19 at the fundamental and second harmonic stopbands.

(a) Fundamental stop-band: (s = .5, N = 0)

At the fundamental stop-band s = .5, N = 0. Using $\alpha_0 = -1/2$ from Equation (71a) in Equations (70) we get the relevant A-matrix elements:

$$A_{11} = -j\left|\frac{\Delta v}{v}\right| \cdot \frac{\pi}{2}\left[\cos\Delta + \frac{P_{.5}(-\cos\Delta)}{P_{-.5}(-\cos\Delta)}\right] \tag{72a}$$

$$A_{13} = 2j\left|\frac{\Delta v}{v}\right| \frac{1}{P_{-.5}(-\cos\Delta)} \tag{72b}$$

$$A_{31} = -j\omega(\epsilon_p + \epsilon_0)W \cdot \frac{\pi}{2}\left[P_{.5}(\cos\Delta) + \frac{P_{-.5}(\cos\Delta)P_{.5}(-\cos\Delta)}{P_{-.5}(-\cos\Delta)}\right] \tag{72c}$$

$$A_{33} = 2j\omega(\epsilon_p + \epsilon_0)W \cdot \frac{P_{-.5}(\cos\Delta)}{P_{-.5}(-\cos\Delta)} \tag{72d}$$

Here, the Legendre polynomials $P_1(\cos\Delta) = \cos\Delta$ and $P_0(\cos\Delta) = 1$ have been used. From Equations (64) we now write the reflection coefficient for the open- and short-circuited array by setting $Z=\infty$ and $Z=0$ respectively.

$$S_{11}\Big|_{Z=\infty} = A_{11} - \frac{A_{13}\,A_{31}}{A_{33}}$$

$$= j\left|\frac{\Delta v}{v}\right| \frac{\pi}{2} \cdot \left[(-\cos\Delta) + \frac{P_{.5}(\cos\Delta)}{P_{-.5}(\cos\Delta)}\right] \tag{73a}$$

$$S_{11}\Big|_{Z=\infty} = A_{11}$$

$$= -j\left|\frac{\Delta v}{v}\right| \frac{\pi}{2} \left[\cos\Delta + \frac{P_{.5}(-\cos\Delta)}{P_{-.5}(-\cos\Delta)}\right] \tag{73b}$$

Equations (73) provide the reflection coefficient of an open- and short-circuited array at the fundamental stop-band as a function of metallization ratio. These agree with the plots in Ref. 19

(b) Second Harmonic stop-band: (s=1, N=0)

For the second harmonic stop-band we may use s=0, N=1 or s=1, N=0; either choice yields the same result. In this case $A_{13}= 0$ so that S_{11} is independent of the load Z which is expected intuitively. We have for the second harmonic stop-band,

$$S_{11} = A_{11}$$

$$= j\left|\frac{\Delta v}{v}\right| \cdot \frac{\pi}{2} \sin^2\Delta \tag{74}$$

for all Z.

E. Summary:

The scatter matrix of a single strip in a periodic array has been derived analytically for all frequencies and metallization ratios. Analytical expressions for the reflection coefficient of a strip in an open- and in a short-circuited array at the fundamental and second harmonic stop-bands are derived as special cases of the general results.

5. ELEMENT FACTOR FOR PERIODIC TRANSDUCER:

A. Introduction:

A large number of practical transducers are modeled as a periodic array of metallic strips with arbitrary impressed voltages. It has been shown[21,22] that the response of such periodic transducer is written as the product of an "element factor" and an "array factor". The element factor was obtained in Ref. 21 using the numerical tables of Ref. 23 which take the effects of two neighboring electrodes into account. In this paper analytical expressions for the element factor are obtained for all frequencies and metallization ratios with the effects of all neighboring electrodes accounted for. The response of the periodic transducer (neglecting regeneration and reflection) is thus obtained analytically for all frequencies.

We first consider a phased array transducer (Fig. 13) in which the voltages on all the electrodes have the same magnitude V but the phase

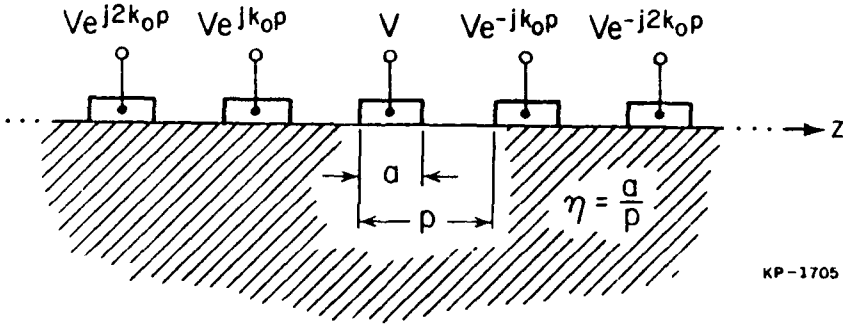

Fig. 13. A phased array transducer with a uniform phase progression of $k_o p$ per period.

progresses uniformly along the array at the rate of $k_o p$ per period where p is the period. The voltage on the n^{th} electrode, V_n is written as,

$$V_n = V \exp(-jnk_o p)$$

$$= V \exp(-jn2\pi s_o) \qquad (75)$$

where s_o is a dimensionless variable related to k_o by,

$$s_o = k_o p/2\pi \tag{76}$$

It will be noticed from Equation (75) that adding any integer to s_o yields the same electrode voltages so that we may without loss of generality restrict the values of s_o such that

$$0 < s_o < 1 \tag{77}$$

The charge distribution in this transducer is known to be[24]

$$Q(\theta) = \frac{2V}{p} (\epsilon_p + \epsilon_o) \cdot \frac{\sin\pi s_o}{P_{s_o - 1}(-\cos\Delta)} \sum_{n=-\infty}^{\infty} P_n(\cos\Delta)\, e^{-j(s_o + n)\theta} \tag{78}$$

where (1) θ is a dimensionless variable related to z by

$$\theta = \frac{2\pi z}{p}$$

(2) ϵ_p is the effective permittivity of the substrate and ϵ_o is the permittivity of the medium above the surface,

(3) $\Delta = \eta\pi$

η being the metallization ratio and

(4) P_ν is the Legendre function of order ν (integer or non-integer).

From Equation (78) we note that the Fourier transform $\bar{Q}(s)$ of $Q(\theta)$ has delta function components at all s given by $s = s_o + n$, n being an integer.

$$\bar{Q}(s) = \bar{Q}(s_o) \cdot P_n(\cos\Delta) \tag{79a}$$

where $s = s_o + n$

and $$\bar{Q}(s_o) = \frac{2V}{p} (\epsilon_p + \epsilon_o) \frac{\sin\pi s_o}{P_{s_o - 1}(-\cos\Delta)} \tag{79b}$$

Here s is the usual spatial harmonic k scaled by $p/2\pi$ to make it dimensionless. Fig. 14 shows a plot of $\bar{Q}(s)$ against s for the phased array transducer with electrode voltages given by (75).

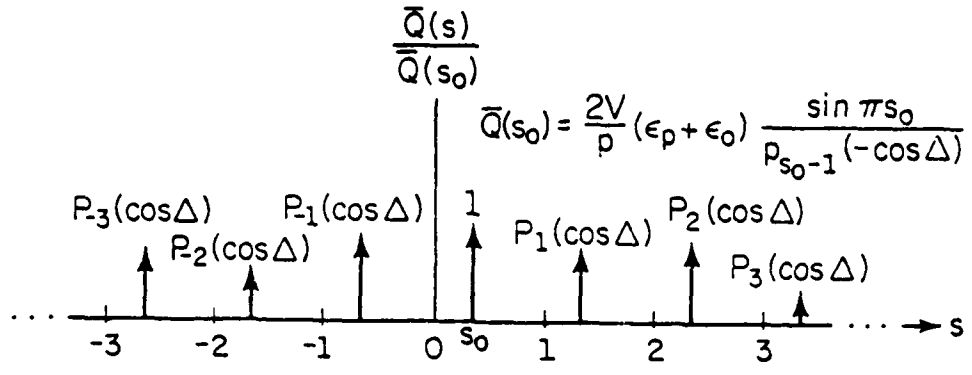

Fig. 14. Fourier transform of charge distribution for a phased array transducer.

The electrode current at each strip has the same magnitude but with a phase progression along the array. The current, D_n at the n^{th} strip is written as

$$D_n = D_o \exp(-js_o 2\pi m) \tag{80a}$$

where: D_o is obtained by integrating $j\omega Q(\theta)$ over the width of a strip

$$D_o = j\omega W \int_{-\Delta}^{+\Delta} d\theta \; Q(\theta)$$

$$= j\omega W \; (\epsilon_p + \epsilon_o) \; . \; 2V \sin\pi s_o \frac{P_{s_o-1}(\cos\Delta)}{P_{s_o-1}(-\cos\Delta)} \tag{80b}$$

W is the length of a strip in the direction perpendicular to the wave propagation.

Now, we wish to determine the charge distribution in a single tap transducer (Fig. 15) since this yields the element factor.[21,22] It is easily seen that this is obtained by superposing the charge distributions in an infinite number of phased array transducers each with V = 1, but with s_o varying uniformly from 0 to 1. The voltage on the n^{th} electrode is then obtained from Equation (75) as,

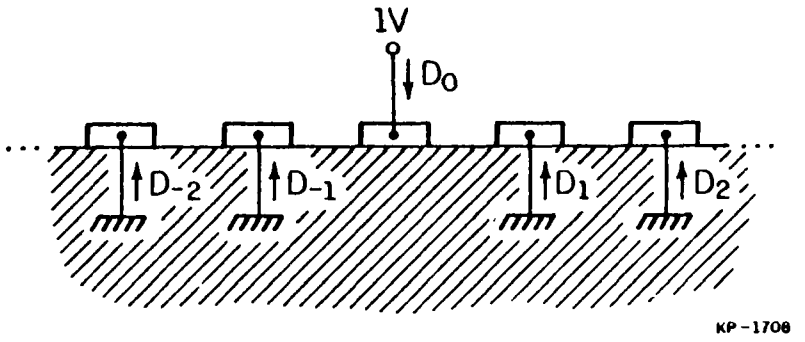

Fig. 15. Electrode currents in a single tap transducer.

$$V_n = \int_o^1 ds_o \exp(-jn2\pi s_o)$$

$$= 1 \quad \text{for } n = 0$$

$$= 0 \quad \text{for } n \neq 0$$

which clearly describes the single tap structure in Fig. 15.

Hence the Fourier transform of the charge distribution in a single tap structure is a continuous function of s given by,

$$\bar{\sigma}(s,\Delta) = \frac{2(\epsilon_p + \epsilon_o)}{p} \frac{\sin\pi s_o}{P_{s_o-1}(-\cos\Delta)} \cdot P_n(\cos\Delta) \qquad (81)$$

where $s = s_o + n$

such that $0 < s_o < 1$ and n is an integer. Fig. 16 shows $s^{1/2}\,\bar{\sigma}\,(s,\Delta)$ plotted against 2s, for different values of the metallization ratio. These agree reasonably with the numerical plots in Fig. 15 of Ref. 21 where 2s corresponds to f/f_o. The discrepancies are possible because only two nearest neighbors were accounted for in the numerical method.

The capacitance of periodic transducers was obtained in Ref. 21 in terms of the electrode currents, D_n (Fig. 15) in the single tap transducer. These are readily obtained from Equation (80) by integrating over s_o from 0 to 1.

$$D_n = 2j\omega W(\epsilon_p + \epsilon_o) \cdot \int_o^1 \sin\pi s_o \frac{P_{s_o-1}(\cos\Delta)}{P_{s_o-1}(-\cos\Delta)} e^{-jn2\pi s_o} ds_o \qquad (82)$$

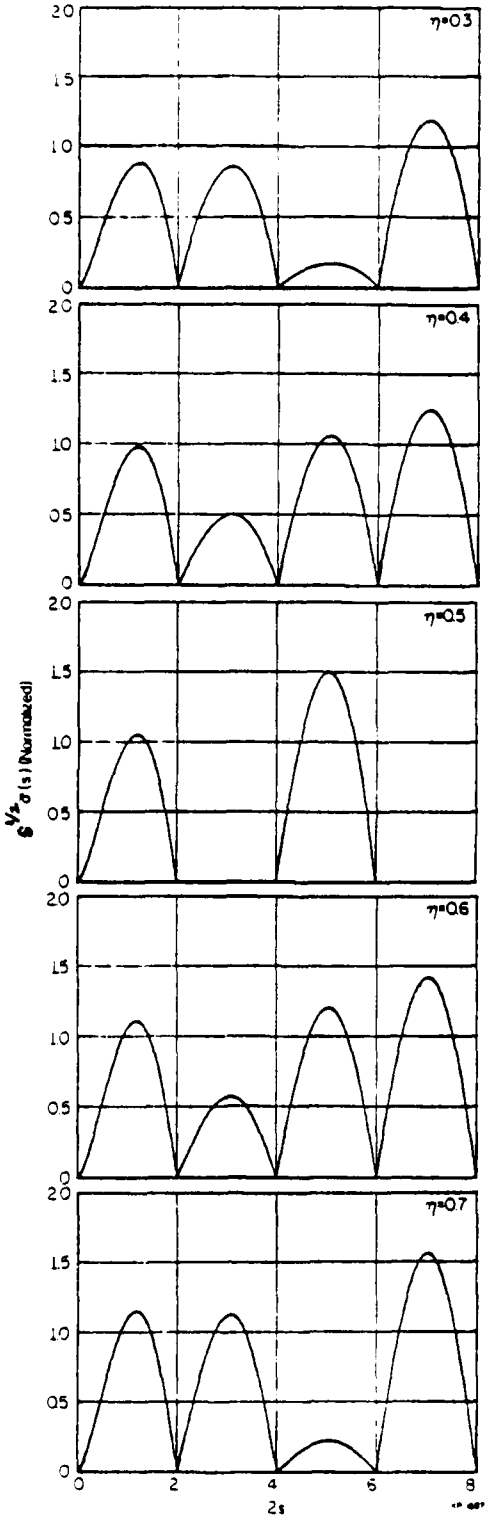

Fig. 16. Element factor for different metallization ratios.

In general the integral has to be obtained numerically. But for $\eta = .5$, $\cos\Delta = 0$; so that $P_{s_o-1}(\cos\Delta) = P_{s_o-1}(-\cos\Delta)$. D_n is then obtained analytically as,

$$D_o = j\omega W (\epsilon_p + \epsilon_o) \frac{4}{\pi} \tag{83a}$$

$$D_n = \frac{D_o}{1 - 4n^2} \tag{83b}$$

It is seen that while D_o is positive, all other D_n's are negative as expected. It may be shown that, as expected, the sum of all the electrode currents is zero.

$$\sum_{n=-\infty}^{\infty} D_n = 0$$

B. Summary:

In Ref. 21 the conductance and capacitance of a periodic transducer with arbitrary voltages were related to the charge distribution and the electrode currents in a single tap transducer. However, these quantities were obtained from numerical tables that take only two nearest neighbors into account. In this section the charge distribution and the electrode currents in a single tap transducer are obtained analytically considering the effects of all the nearest neighbors, making the analysis more accurate and more convenient. The overall charge distribution in a periodic transducer is given by Equation (5) of Ref. 21 as the product (in k-space) or the convolution (in x-space) of the voltage distribution and basic charge distribution function (BCDF); the BCDF is now known exactly from Equation (81).

REFERENCES

1. A. J. Slobodnik, Jr., K. R. Laker, T. L. Szabo, W. J. Kearns, and G. A. Roberts, "Low Sidelobe SAW Filters Using Overlap and Withdrawal Weighted Transducers," 1977 Ultrasonics Symposium Proceedings, p., 757.

2. B. A. Auld, "Acoustic Fields and Waves in Solids," Vol. II, Wiler-Interscience 1973, p., 275-283 and p., 302-309.

3. B. A. Auld, "Acoustic Fields and Waves in Solids," Vol. II, Wiley-Interscience 1973, p., 178-180.

4. C. Dunnrowicz, F. Sandy, T. Parker, "Reflection of Surface Waves from Periodic Discontinuities," 1976 Ultrasonics Symposium Proceedings, IEEE Cat. No. 76CH1120-5SU.

5. S. Datta and B. J. Hunsinger, "Analysis of Surface Waves Using Orthogonal Functions," J. Appl. Phys. 49, (2), Feb. 1978, p., 475-479.

6. R. C. M. Li and J. Melngailis, "The Influence of Stored Energy at Step Discontinuities on the Behavior of Surface-Wave Gratings," IEEE Transactions, SU-22, No. 3, May 1975.

7. S. D. Wu and H. S. Tuan, "Rayleigh Wave Reflection from a Groove in Y-Z $LiNbO_3$: A perturbation approach," J. Appl. Phys. 50, 1, Jan. 1979.

8. D. A. Simons, "Reflection of Rayleigh Waves by Strips, Grooves, and Periodic Arrays of Strips or Grooves," J. Acoust. Soc. Am. 63, 1292, May 1978.

9. S. Datta and B. J. Hunsinger, "First-Order Reflection Coefficient of Surface Acoustic Waves from Thin Strip Overlays," J. Appl. Phys. 50, 5661, Sept. 1979.

10. R. A. Collins, "Field Theory of Guided Waves," McGraw-Hill, 1960, p., 368-371.

11. B. A. Auld, "Acoustic Fields and Waves in Solids," Vol. II, Wiley Interscience 1973, p., 275-283.

12. See reference 6, p., 302-309.

13. W. J. Tanski, "Developments in Resonators on Quartz," 1977 Ultrasonics Symposium Proceedings, IEEE Cat. #77CH1264-1SU, p., 900.

14. J. Melngailis and R. C. Williamson, "Interaction of Surface Waves and Bulk Waves in Gratings," 1978 Ultrasonics Symposium Proceedings, IEEE Cat. #78CH1344-1SU, p., 623.

15. K. Blotekjaer, K. A. Ingebrigtsen and H. Skeie, "A Method for Analyzing Waves in Structures Consisting of Metal Strips on Dispersive Media," IEEE Trans., Vol. ED-20, No. 12, Dec. 1973.

16. K. Blotekjaer, K. A. Ingebrigtsen and H. Skeie, "Acoustic Surface Waves in Piezoelectric Materials with Periodic Metal Strips on the Surface," IEEE Trans., Vol. ED-20, No. 12, Dec. 1973.

17. T. Aoki and K. A. Ingebrigtsen, "Equivalent Circuit Parameters of Interdigital Transducers Derived from Dispersion Relations for Surface Acoustic Waves in Periodic Metal Gratings," IEEE Trans.,Vol. SU-24, No. 3, May 1977.

18. T. Aoki and K. A. Ingebrigtsen, "Acoustic Surface Waves in Split Strip Periodic Metal Gratings on a Piezoelectric Surface," IEEE Trans., Vol. SU-24, No. 3, May 1977.

19. T. Aoki and S. Hattori, "Equivalent Circuit Parameters for Harmonic Operations of SAW Transducers," 1977 Ultrasonics Symposium Proceedings, p., 653.

20. B. A. Auld, Acoustic Fields and Waves in Solids, Vol. II, Wiley and Sons Inc. 1973, p., 306.

21. S. Datta, B. J. Hunsinger and D. C. Malocha, "A Generalized Model for Periodic Transducers with Arbitrary Voltages," IEEE Trans. on Sonics and Ultrasonics, SU-26, 235, May 1979.

22. S. Datta and B. J. Hunsinger, "Redefined Element Factor for Simplified IDT Design," Elect. Lett., 14, (23), November 1978.

23. W. R. Smith and W. F. Pedler, "Fundamental- and Harmonic-Frequency Circuit Model Analysis of Interdigital Transducers with Arbitrary Metallization Ratios and Polarity Sequences," IEEE Trans. Vol. MTT-23, No. 11, November 1975.

24. R. C. Peach and C. Dix, "A Low Loss Medium Bandwidth Filter on Lithium Niobate," IEEE Ultrasonics Symposium 1978.

APPENDIX I: DELTERV and DELTERZ from Scattering Parameters:

In this report the scattering parameters have been derived for a single section in an infinite array. In this appendix, the impedance mismatch ΔZ and the fractional change in velocity $\Delta v/v$ for an equivalent transmission model are derived for the S-parameters.

Let ω be the radian frequency, v_o the unperturbed surface wave velocity, ℓ the length of one section and η the metallization ratio. In the equivalent transmission line model, the metallized sections have an impedance and velocity different from the unmetallized sections (Fig. A1). In addition, two susceptances jB are included at the edges of the metallized section in order to account for the even harmonic reflection which is not predicted by the simple mismatched transmission line model.

A straightforward analysis shows that,

$$S_{11}e^{j\theta} = j[\Delta Z \sin\eta\theta - B\cos\eta\theta] \tag{A1a}$$

$$S_{12}e^{j\theta} = 1 - j\eta\theta\frac{\Delta v}{v} \tag{A1b}$$

where $\theta = \omega\ell/v_o$ and ΔZ, B are normalized to the characteristic impedance. Using these equations ΔZ and $\Delta v/v$ are calculated from S_{11} and S_{12}. It will be noted that at the fundamental with $\eta = .5$, $\cos\eta\theta = 0$; so that B does not enter the picture. On the other hand, at the second harmonic $\sin\eta\theta = 0$ so that ΔZ does not enter the picture. At intermediate frequencies or for η other than .5 there is no unique solution for ΔZ and B; however, it is possible that a particular choice might result in values that are nearly constant with η or with frequency.

DELTERV and DELTERZ are obtained from $\frac{\Delta v}{v}$ and $\frac{\Delta Z}{Z}$ from the relations:[1]

$$\text{DELTERV} = \frac{K^2}{2} + \frac{\Delta v}{v} \tag{A1c}$$

$$\text{DELTERZ} = -\frac{K^2}{2} - \frac{\Delta Z}{Z} \tag{A1d}$$

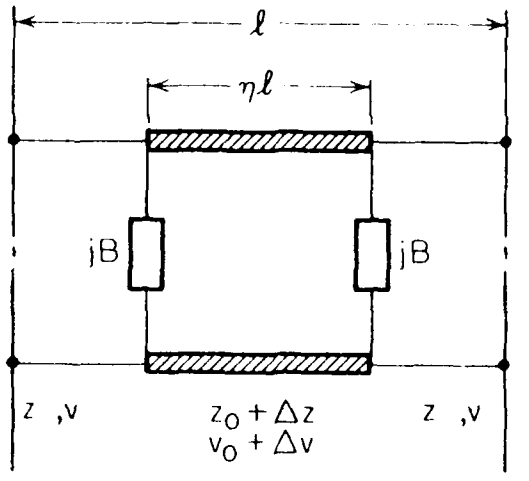

$\theta = \omega\ell/v_0$
η = Metallization Ratio
ω = Radian Frequeny
v_0 = Unperturbed Surface Wave Velocity

KP-1853

Fig. A1. Equivalent transmission line model.

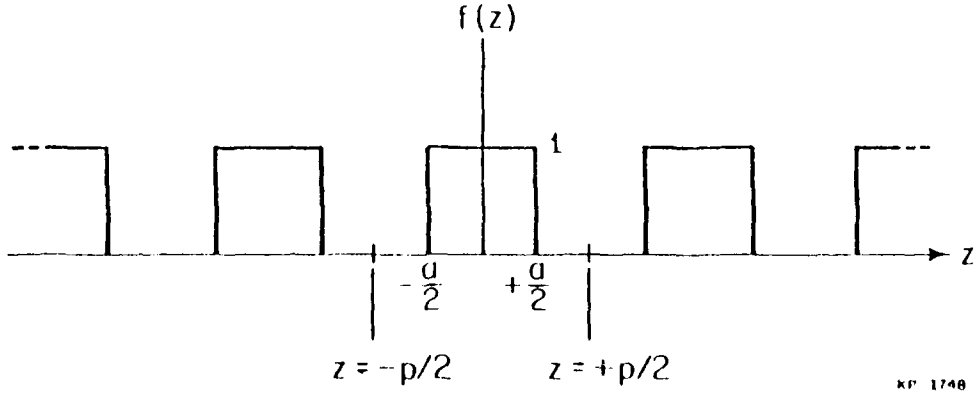

Fig. A2. Function describing geometry of the strips.

APPENDIX II:

In this appendix we will evaluate the stress-displacement relation for a thin periodic array of strips. Let us first consider a particle displacement vector with a single spatial frequency $\beta^{(n)}$.

$$U_i = U_i^{(n)} \exp[-j\beta^{(n)} Z] \tag{A2a}$$

where $\beta^{(n)} = \beta + n \cdot 2\pi/p$

If the thin layer were uniform rather than periodic the stresses τ_i would also have the same spatial frequency $\beta^{(n)}$. The relation between τ and U can then be expressed by a constant matrix $[A^{(n)}]$ such that

$$\tau_i^{(n)} = \sum_{j=x}^{z} A_{ij}^{(n)} U_j^{(n)} , \qquad i = x, y, z \tag{A2b}$$

The matrix elements $A_{ij}^{(n)}$ are known from a first-order perturbation analysis.[6]

$$A_{xx}^{(n)} = \beta^{(n)} (\beta^{(n)}h) [\alpha'_{xx} - \rho'\omega^2/\{\beta^{(n)}\}^2] \tag{A3a}$$

$$A_{xz}^{(n)} = -\beta^{(n)} (\beta^{(n)}h) \alpha'_{xz} \tag{A3b}$$

$$A_{zx}^{(n)} = -\beta^{(n)} (\beta^{(n)}h) \alpha'_{zx} \tag{A3c}$$

$$A_{zz}^{(n)} = \beta^{(n)} (\beta^{(n)}h) [\alpha'_{zz} - \rho'\omega^2/\{\beta^{(n)}\}^2] \tag{A3d}$$

$$A_{yy}^{(n)} = \beta^{(n)} (\beta^{(n)}h) [-\rho'\omega^2/\{\beta^{(n)}\}^2] \tag{A3e}$$

and the other $A_{ij}^{(n)}$ are zero, where ρ' is the mass-density of the strip material, and α'_{xx}, α'_{xz}, α'_{zx}, α'_{zz} have the dimensions of stiffness and are given by,

$$\alpha'_{xx} = S_3^3/D \tag{A4a}$$

$$\alpha'_{xz} = S_5^3/D \tag{A4b}$$

$$\alpha'_{zx} = S^5_3/D \tag{A4c}$$

$$\alpha'_{zz} = S^5_5/D \tag{A4d}$$

$$S^I_J = (S'_{II}S'_{IJ} - S'_{IJ}S'_{II})/S'_{II} \tag{A4e}$$

$$D = S^5_5 S^3_3 - S^3_5 S^5_3 \tag{A4f}$$

[S'] is the compliance tensor of the strip material.

Now if the array of strips is periodic, it has been shown[3,4] that the stress may be written in terms of the particle displacements as,

$$\tau_i(z) = \sum_{j=x}^{z} B^{(n)}_{ij}(z)\, U^{(n)}_i \quad , \qquad i = x, y, z \tag{A5}$$

where

$$B^{(n)}_{xx}(z) = A^{(n)}_{xx}\, f(z) - j\,(\beta^{(n)}h)\,\alpha'_{xx}\,\frac{df}{dz} \tag{A6a}$$

$$B^{(n)}_{xz}(z) = j\,(\beta^{(n)}h)\,\alpha'_{zx}\,\frac{df}{dz} \tag{A6b}$$

$$B^{(n)}_{zx}(z) = j\,(\beta^{(n)}h)\,\alpha'_{zx}\,\frac{df}{dz} \tag{A6c}$$

$$B^{(n)}_{zz}(z) = A^{(n)}_{zz}\, f(z) - j\,(\beta^{(n)}h)\,\alpha'_{zz}\,\frac{df}{dz} \tag{A6d}$$

$$B^{(n)}_{yy}(z) = A^{(n)}_{yy}\, f(z) \tag{A6e}$$

and the other $B^{(n)}_{ij}$ are zero. Here f(z) is a rectangular function describing the geometry of the strips and is shown in Fig. A2. The terms involving $\frac{df}{dz}$ in Equations (A6) represent delta functions at the edges of the strip; the physical origin of these delta functions has been explained in References 3 and 4. Multiplying Equation (A4) by $e^{j\beta^{(m)}z}$, integrating over one period and using text Equations (1b) and 3a) we have,

$$(\beta h) \cdot L_{ij}^{(n,m)} = \frac{1}{p} \int_{-p/2}^{+p/2} B_{ij}^{(n)}(z) \exp[j(\beta^{(m)} - \beta^{(n)})z]\, dz \qquad (A7)$$

Using $B_{ij}^{(n)}(z)$ from Equations (A6), we get $L_{ij}^{(n,m)}$:

$$L_{xx}^{(n,m)} = \beta\left[-\rho' c_s^2 + \alpha'_{xx}\left(1 + \frac{m.2\pi}{\beta p}\right)\left(1 + \frac{n.2\pi}{\beta p}\right)\right] F_{m-n} \qquad (A8a)$$

$$L_{xz}^{(n,m)} = \beta\,\alpha'_{xz}\left(1 + \frac{n.2\pi}{\beta p}\right)\left(1 + (n-m).\frac{2\pi}{\beta p}\right) f_{m-n} \qquad (A8b)$$

$$L_{zx}^{(n,m)} = \beta\,\alpha'_{zx}\left(1 + \frac{n.2\pi}{\beta p}\right)\left(1 + (n-m).\frac{2\pi}{\beta p}\right) f_{m-n} \qquad (A8c)$$

$$L_{zz}^{(n,m)} = \beta\left[-\rho' c_s^2 + \alpha'_{zz}\left(1 + \frac{m.2\pi}{\beta p}\right)\left(1 + \frac{n.2\pi}{\beta p}\right)\right] F_{m-n} \qquad (A8d)$$

$$L_{yy}^{(n,m)} = \beta\left[-\rho' c_s^2\right] F_{m-n} \qquad (A8e)$$

Where,

$$F_{m-n} = \frac{1}{p} \int_{-p/2}^{+p/2} f(z) \exp[j(\beta^{(m)} - \beta^{(n)})z]\, dz$$

$$= \eta \frac{\sin(m-n)\pi\eta}{(m-n)\pi\eta} \qquad (A8f)$$

η is the duty factor = a/p, β is the surface wave wavenumber and c_s is the surface wave velocity. The other $L_{ij}^{(n,m)}$ are zero.

APPENDIX III:

In this appendix we will evaluate the stress-displacement relation for a semi-infinite substrate. As discussed in the paper, the substrate does not introduce any coupling between different spatial harmonics (Equation (5) of the text).

Let us consider a particle displacement vector with a single spatial frequency $\beta^{(n)} = \beta + n.2\pi/p$. If we assume that the particle displacements decay into the bulk from their surface values given by (A9) as an exponential

$e^{-\alpha y}$, then from the field equations we get three values of α. These correspond to three elastic modes of the solid. The field equation is written as,

$$\sum_{j,k,\ell\ 1}^{3} C_{ijk\ell} \frac{\partial^2 u_k}{\partial x_j \partial x_\ell} = \rho\omega^2 u_i \qquad \text{(A9)}$$

where, C is the stiffness tensor and ρ, the mass density of the substrate. The coordinates x_1, x_2, x_3 are used in place of x, y, z for convenience. If we replace the derivative operators by,

$$\partial/\partial x_1 \rightarrow 0$$

$$\partial/\partial x_2 \rightarrow \alpha$$

$$\partial/\partial x_3 \rightarrow j\beta^{(n)}$$

Equation (A9) becomes an algebraic equation. The determinant is a sixth order polynomial in α, so that by setting it equal to zero we get six values of α of these three represent exponentially growing solutions and are rejected. Corresponding to each of the other three $\alpha^{(1)}$, $\alpha^{(2)}$, $\alpha^{(3)}$ we get particle displacement vectors whose surface values are $\{u^{(1)}\}$, $\{u^{(2)}\}$ and $\{u^{(3)}\}$. The total particle displacement $\{U\}$ at the surface is a linear combination of these.

$$\{U\} = [u] \cdot \{A\} \qquad \text{(A10)}$$

where, $[u]$ is the matrix formed by arranging $\{u^{(1)}\}$, $\{u^{(2)}\}$, and $\{u^{(3)}\}$ in columns. $\{A\}$ is a vector whose components A_1, A_2, A_3 are constants representing the linear combination.

Now corresponding to each solution $\{u^{(1)}\}$, $\{u^{(2)}\}$, $\{u^{(3)}\}$, we may calculate the stress vector at the surface $\{T^{(1)}\}$, $\{T^{(2)}\}$, $\{T^{(3)}\}$. the

total stress, τ is written as a linear combination of these.

$$\{\tau\} = [T]\ \{A\} \tag{A11}$$

Combining (A10) and (A11),

$$\{\tau\} = [T]\ [u]^{-1}\ \{U\} \tag{A12}$$

comparing with text Equation (3b).

$$[S] = [T]\ [u]^{-1} \tag{A13}$$

The procedure outlined here may be used for any anisotropic substrate to obtain the matrix $[S^{(n,n)}]$ relating the stress and displacement at a given spatial frequency $\beta^{(n)}$. For an isotropic substrate it is possible to obtain analytical expressions for the matrix elements. The three values of α are obtained as,

$$\alpha^{(1)} = \alpha_L = (\{\beta^{(n)}\}^2 - k_L^2)^{1/2} \tag{A14a}$$

$$\alpha^{(2)} = \alpha_S = (\{\beta^{(n)}\}^2 - k_S^2)^{1/2} \tag{A14b}$$

$$\alpha^{(3)} = \alpha_S = (\{\beta^{(n)}\}^2 - k_S^2)^{1/2} \tag{A14c}$$

where,

$$k_L^2 = \frac{\omega^2 \rho}{\lambda + 2\mu} \tag{A15a}$$

$$k_S^2 = \frac{\omega^2 \rho}{\mu} \tag{A15b}$$

where λ and μ are the Lame' constants of the substrate. The matrix [u] is given by,

$$[u] = \begin{bmatrix} -j\beta^{(n)} & 0 & 0 \\ 0 & j\beta^{(n)} & \alpha^{(1)} \\ 0 & \alpha^{(2)} & -j\beta^{(n)} \end{bmatrix} \tag{A16}$$

The [T] matrix is obtained as,

$$[T] = \mu \begin{bmatrix} -j\beta^{(n)}\alpha^{(3)} & 0 & 0 \\ 0 & 2j\beta^{(n)}\alpha^{(2)} & 2\{\beta^{(n)}\}^2 - k_S^2 \\ 0 & 2\{\beta^{(n)}\}^2 - k_S^2 & -2j\beta^{(n)}\alpha^{(3)} \end{bmatrix} \tag{A17}$$

From (A16) and (A17) we get the [S]-matrix.

$$S_{xx}^{(n,n)} = \mu \alpha_S \tag{A18a}$$

$$S_{yy}^{(n,n)} = \frac{\mu \alpha_S k_S^2}{\{\beta^{(n)}\}^2 - \alpha_L \alpha_S} \tag{A18b}$$

$$S_{yz}^{(n,n)} = j\mu\beta^{(n)} \frac{\alpha_S^2 + \{\beta^{(n)}\}^2 - 2\alpha_L\alpha_S}{\{\beta^{(n)}\}^2 - \alpha_L\alpha_S} \tag{A18c}$$

$$S_{zy}^{(n,n)} = -S_{yz}^{(n,n)} \tag{A18d}$$

$$S_{zz}^{(n,n)} = \frac{\mu \alpha_L k_S^2}{\{\beta^{(n)}\}^2 - \alpha_L \alpha_S} \tag{A18e}$$

The other $S_{ij}^{(n,n)}$ are zero. For an arbitrary anisotropic substrate analytical expressions are not obtainable, but the matrix elements are numerically evaluated for a given $\beta^{(n)}$ using the procedure outlined above.

APPENDIX IV:

In this appendix the values of α_m are derived so as to satisfy equations (7) and (8):

$$e^{-jN\theta} + \sum_{m=0}^{N+1} \alpha_m \sum_{n=-\infty}^{\infty} S_n P_{n+m-N-1}(\cos\Delta) e^{-jn\theta} = 0 \qquad |\theta| < \Delta \tag{A19}$$

$$\sum_{m=0}^{N+1} \alpha_m \sum_{n=-\infty}^{\infty} P_{n+m-N-1}(\cos\Delta) e^{-jn\theta} = 0 \qquad \Delta < |\theta| < \pi \tag{A20}$$

It is known from the properties of the Legendre polynomial that[1],

$$\sum_{n=-\infty}^{\infty} S_{n-m} P_{n-m}(\cos\Delta) e^{-jn\theta} = 0 \qquad |\theta| < \Delta \tag{A21}$$

$$\sum_{n=-\infty}^{\infty} P_{n-m}(\cos\Delta) e^{-jn\theta} = 0 \qquad \Delta < |\theta| < \pi \tag{A22}$$

where m is any integer. From (A4) it is seen that (A2) is satisfied for any choice of α_m's.

In order to satisfy (A1) we choose α_m's such that,

$$e^{-jN\theta} + \sum_{m=0}^{N+1} \alpha_m \sum_{n=-\infty}^{\infty} S_n P_{n+m-N-1}(\cos\Delta) e^{-jn\theta}$$

$$= \sum_{m=0}^{N+1} \alpha_m \sum_{n=-\infty}^{\infty} S_{n+m-N-1} P_{n+m-N-1}(\cos\Delta) e^{-jn\theta} \tag{A23}$$

From equation (A3) we note that the right hand side is 0 for $|\theta| < \Delta$. Equation (A5) yields,

$$e^{-jN\theta} + \sum_{m=0}^{N+1} \alpha_m \beta_m = 0 \qquad |\theta| < \Delta \tag{A24}$$

where,

$$\beta_m = \sum_{n=-\infty}^{+\infty} \left(S_n - S_{n-(N+1-m)} \right) P_{n+m-N-1}(\cos\Delta) e^{-jn\theta}$$

$$= 0 \qquad \text{if } m = N + 1$$

$$= 2 \sum_{n=0}^{N-m} P_{n+m-N-1}(\cos\Delta)e^{-jn\theta} \qquad \text{if } m < N + 1$$

Since $\hat{P}_{N+1} = 0$ it is apparent from Equation (A6) that α_{N+1} can have any arbitrary value. Leaving this term out,

$$e^{-jN\theta} = \sum_{m=0}^{N} 2\alpha_m \sum_{n=0}^{N-m} P_{n+m-N-1}(\cos\Delta)e^{-jn\theta} = 0$$

i.e. $$e^{-jN\theta} + 2\sum_{m=0}^{N} e^{-jn\theta} \sum_{n=0}^{N-n} \alpha_m P_{n+m-N-1}(\cos\Delta) = 0$$

Equation each power ($e^{-j\theta}$) to 0 starting from $e^{-jN\theta}$ we get,

$$\alpha_0 = -1/2 \tag{A25}$$

$$\sum_{m=0}^{\ell} \alpha_m P_{m-\ell-1}(\cos\Delta) = 0, \quad \ell = 1 \text{ to } N \tag{A26}$$

Equation (A7) is written as,

$$\alpha_\ell = -\sum_{m=0}^{\ell-1} \alpha_m P_{\ell-m}(\cos\Delta), \quad \ell = 1 \text{ to } N \tag{A27}$$

noting that $P_{-1}(\cos\Delta) = 1$ and $P_{m-\ell-1} = P_{\ell-m}$.

APPENDIX V:

In this appendix the terminal voltage and current at a strip are determined from the tangential electric field and the normal electrical displacement. From Equations (5a), (7c) and (8),

$$E_z(\vartheta) = j\frac{2\pi}{p}(s+N)\mathfrak{D}_+ e^{-js\theta}\left[e^{-jN\theta} + \sum_{m=0}^{N+1} \alpha_m \sum_{n=-\infty}^{\infty} S_n P_{n+m-N-1}(\cos\Delta)e^{-jn\theta}\right]$$

$$= j\frac{2\pi}{p}(s+N)\mathfrak{D}_+ \cdot \sum_{m=0}^{N+1} \alpha_m \sum_{n=-\infty}^{\infty} S_{n+m-N-1} P_{n+m-N-1}(\cos\Delta)e^{-j(s+n)\theta} \tag{A28}$$

where Equation (A5) has been used.

Integrating (A9),

$$\phi(\theta) = (s+N)\phi_+ \sum_{m=0}^{N+1} \alpha_m \sum_{n=-\infty}^{\infty} \frac{S_{n+m-N-1} P_{n+m-N-1}(\cos\Delta)}{s+n} e^{-j(s+N)\theta}$$

Since the potential is uniform over a strip, the strip voltage V is equal to $\phi(0)$.

$$V = (s+N)\phi_+ \sum_{m=-}^{N+1} \alpha_m \sum_{n=-\infty}^{\infty} \frac{S_{n+m-N-1} P_{n+m-N-1}(\cos\Delta)}{s+n}$$

$$= (s+N)\phi_+ \sum_{m=0}^{N+1} \frac{\alpha_m \cdot (-1)^{N+1-m} \pi P_{N-m+s}(-\cos\Delta)}{\sin\pi s} \qquad \text{(A29)}$$

using the derivation in Ref. 7. The strip current is obtained by integrating $D_y(\theta)$ over one strip width. From Equation (10),

$$I = j\omega(\epsilon_p + \epsilon_0)(s+N)\phi_+ \sum_{m=0}^{N+1} \alpha_m \int_{-\Delta}^{+\Delta} \sum_{n=-\infty}^{\infty} P_{n+m-N-1}(\cos\Delta) e^{-j(s+n)\theta}$$

$$= j\omega(\epsilon_p + \epsilon_0)(s+N)\phi_+ \sum_{m=0}^{N+1} \alpha_m \cdot 2\pi P_{N-m+s}(\cos\Delta) \qquad \text{(A30)}$$

again using the result in Ref. 7.

APPENDIX VI:

In this appendix the following integral used in Equation (20) is computed:

$$J = \int_{-\pi}^{+\pi} d\theta \sum_{n=-\infty}^{\infty} P_{n+m-N-1}(\cos\Delta) e^{-j(2s+n+N)\theta}$$

We have, $J = \sum_{n=-\infty}^{\infty} P_{n+m-N-1}(\cos\Delta) \cdot \frac{2\sin\pi(2s+n+N)}{(2s+n+N)}$

$$= 2 \sin 2s\pi \cdot \sum_{n=-\infty}^{\infty} (-1)^{n+2N-m+1} \frac{P_n(\cos\Delta)}{2s+n+2N-m+1}$$

$$= 2\sin 2s\pi \cdot (-1)^{2N-m+1} \cdot \sum_{n=0}^{\infty} (-1)^n P_n(\cos\Delta) \left[\frac{1}{n+2s+2N-m+1} - \frac{1}{2N+2s-n-m}\right]$$

$$= 2\sin 2s\pi \cdot (-1)^{2N-m} P_{2N+2s-m}(\cos\Delta) \cdot \frac{\pi}{\sin\pi(2N+2s-m)}$$

using the definition of Legendre functions P_γ for non-integer γ.

This yields,

$$J = 2\pi \cdot P_{2N+2s-m}(\cos\Delta) \qquad \text{(A31)}$$

MISSION
of
Rome Air Development Center

RADC plans and executes research, development, test and selected acquisition programs in support of Command, Control Communications and Intelligence (C^3I) activities. Technical and engineering support within areas of technical competence is provided to ESD Program Offices (POs) and other ESD elements. The principal technical mission areas are communications, electromagnetic guidance and control, surveillance of ground and aerospace objects, intelligence data collection and handling, information system technology, ionospheric propagation, solid state sciences, microwave physics and electronic reliability, maintainability and compatibility.

Printed by
United States Air Force
Hanscom AFB, Mass. 01731

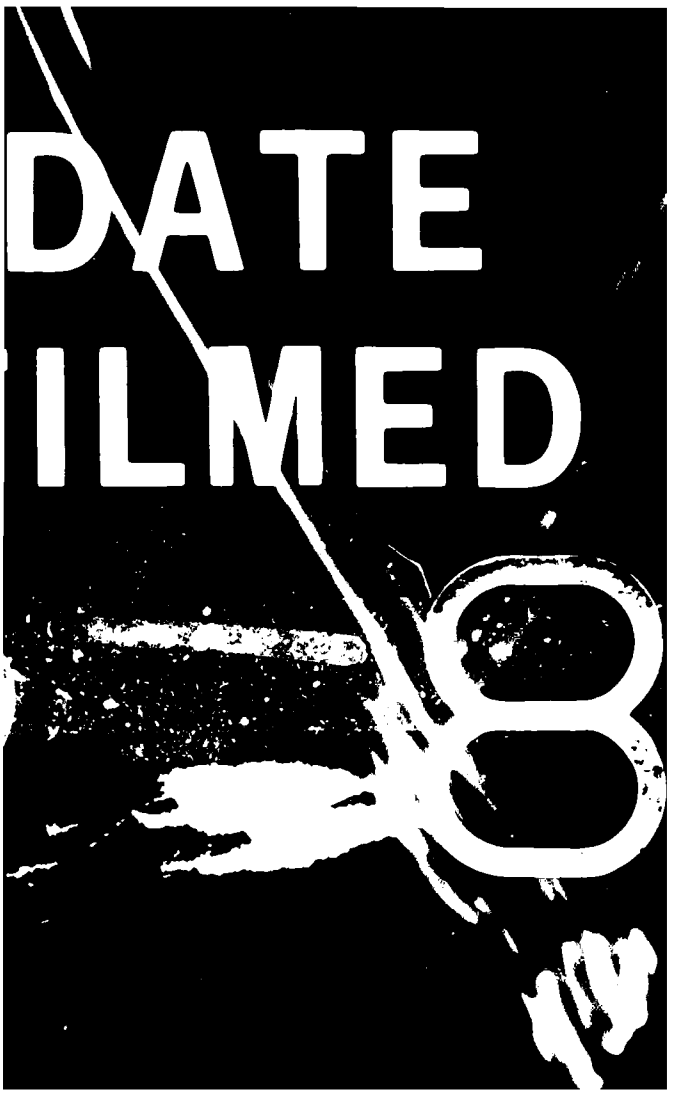
DATE
ILMED

AD-A097 337 ILLINOIS UNIV AT URBANA COORDINATED SCIENCE LAB F/G 9/3
TERMINATION OF SURFACE ACOUSTIC WAVE VELOCITY AND IMPEDANCE DIF--ETC(U)
FEB 81 B J HUNSINGER, S DATTA F19628-78-C-0040
UNCLASSIFIED RADC-TR-81-4 NL

SUPPLEMENTA

INFORMATION

ERRATA

8 April 1981

RADC-TR-81-4, Termination of Surface Acoustic Wave Velocity and Impedance Differences Between Metal Strips and Free Surface Regions of Metallic Gratings
February 1981

The title of above RADC TR should be corrected to read:

Research to Provide a Theoretical Determination of Surface Acoustic Wave Velocity and Impedance Differences Between Metal Strips and Free Surface Regions of Metallic Gratings.

Rome Air Development Center
Air Force Systems Command
Griffiss Air Force Base, New York 13441

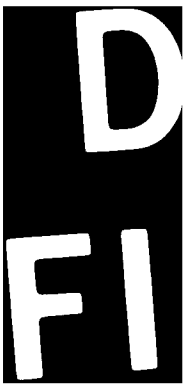
D
FI